DESIGN AND IMPLEMENTATION OF A PLASMA ENHANCED CHEMICAL VAPOUR DEPOSITION (PECVD) SYSTEM FOR THE STUDY OF C_{60}-POLYMER COMPOSITE THIN FILMS AND SURFACE FUNCTIONALIZATION EFFECTS ON C_{60}

By

Amna Tariq

Under the Supervision of Prof. Sylvain Coulombe and Prof. J.-L. Meunier

Department of Chemical Engineering
McGill University, Montreal

June 2004

A thesis submitted to the Faculty of Graduate Studies and Research in partial fulfillment of the requirements of the degree of Masters of Engineering

Your file Votre référence
ISBN: 0-494-06589-3
Our file Notre référence
ISBN: 0-494-06589-3

TARA TARIQ

" ... It is not having been in the dark house, but having left it that counts ..."
- Theodore Roosevelt

ABSTRACT

The current trend of developing nanophase materials motivates the development of production techniques for nanometer-scale structures for the Si-based semiconductor industry, biomedical research and electro-optics. Nanocomposite (NC) coatings are the latest interest as their properties differ greatly from microcrystalline films with fields of application covering magnetic, optical, electronic, mechanical and oxidation resistance properties. An innovative concept of using coated nanoparticles (NP) as a precursor material for improved NCs is emerging. Nanometric sized particles are remarkably taxing to handle due to their inclination to aggregate. A considerable obstacle in NC thin film production via plasma enhanced chemical vapour deposition (PECVD) is the controlled introduction of nano-sized filler material into the plasma processing reactor and its eventual incorporation into the polymer matrix.

This research project aimed at the development of a PECVD process for the deposition of C_{60}-PPPE (plasma polymerized polyethylene) NC thin films. A continuous throughput PECVD system was designed for the co-deposition of a polymer matrix and C_{60} particles, in effect, yielding composite thin films on 1" quartz and silicon substrates. In this process, the C_{60} molecules are sublimated from their solid powder form, transported to the plasma chamber, pre-coated in-flight before being dispersed and co-deposited in the polymeric matrix. The plasma polymerization of ethane in the low pressure, radio frequency (RF) plasma was studied with a mapping of the polymer thin film growth at various deposition times. Percentage coverage of C_{60} films was studied at several sublimation temperatures ranging from 500 – 750 °C. Compositional studies of PPPE and C_{60} films obtained were carried out using FPA-FTIR. The surface morphology and topography of composite films was analyzed using OM and FESEM. Furthermore, samples of C_{60} deposited in the reactor were analyzed via TEM for possible deagglomeration and nanocoatings.

Within the operating conditions employed in this study, it was shown that the sublimation of C_{60} followed by exposure to a glow discharge does not lead to fragmentation of the molecules. Also, the sublimed clusters have low impact energy on the substrate surface, hence yielding *sooty* films. Furthermore, it is shown that the plasma environment does not promote the re-agglomeration of the particles due to the in situ build up of surface charges. Finally, observations made with SEM and TEM show a rapid functionalization of the C_{60} clusters when exposed to an ethane plasma and consequently acquired an organic thin film. This novel in-flight nanoparticle surface treatment process leads to a reduction of the nanoparticle surface energy once liberated from the raw material source thereby promoting nanoscale cluster formation, and nanostructured film formation.

RÉSUMÉ

L'intérêt croissant porté aux matériaux nanophasés motive les développements de techniques de production adaptées à l'industrie des semiconducteurs, la recherche biomédicale et l'optique-électronique. Les revêtements nano-composites (NC) dont les propriétés diffèrent considérablement de celles des couches minces microcrystallines émergent comme nouveaux matériaux ayant des propriétés magnétiques, optiques, électroniques, mécaniques et de résistance à l'oxidation. Une des approches prometteuses pour la fabrication de ces nano-composites est l'utilisation comme précurseur à la formation du composite de nanoparticules enrobées. Toutefois, en raison de leur tendance naturelle à l'agglomération, les nanoparticules se manipulent avec grande difficulté. Ce dernier obstacle rend difficile l'introduction bien contrôlée du matériau nanométrique dans le réacteur de déposition réactive assistée par plasma (acronyme anglais : PECVD), ainsi que la dispersion de ce matériau dans une couche mince en formation.

Ce projet de recherche a comme thème principal le développement d'un processus PECVD pour la déposition de couches minces nano-composites C_{60}-matrice polymérique de PPPE (polyéthylène polymérisé par plasma). Un système PECVD à écoulement continu a été conçu pour la co-déposition de C_{60} et d'une couche mince polymérique sur un substrat immobile de silicium ou de quartz. Dans ce procédé, les molécules de C_{60} sont libérées par sublimation d'une source solide, transportées et enrobées d'une couche mince au sein d'un plasma réactif entretenu par couplage radio-fréquentiel à basse pression et dispersées au sein d'une couche mince en formation sur le substrat. La polymerisation par plasma de l'éthane a été étudiée en premier lieu et le taux de croissance du film en fonction du temps de déposition fût obtenu. Ensuite, le taux de couverture des films de C_{60} a été obtenu en fonction de la température de sublimation des C_{60}.

Les principales conclusions de cette étude sont les suivantes. D'abord, les molécules de C_{60} ne sont pas fragmentées lors de leur passage dans le plasma de la décharge électroluminescente. Les *clusters* de C_{60} formés en phase gazeuse suivant leur sublimation frappent le substrat à faible énergie, donnant ainsi lieu à la formation de couches *poudreuses*. Le milieu plasma limite la ré-agglomération des particules en raison de la formation d'une charge répulsive en surface. Finalement, les observations réalisées avec l'aide de microscopes électroniques à balayage et à transmission des électrons revèlent qu'un traitement de surface dans un plasma d'éthane donne lieu à une fonctionalisation rapide de la surface et à la formation d'un couche mince de nature organique. Ce nouveau procédé permet donc de réduire l'énergie de surface des particules sublimées et de favoriser la formation de *clusters* de taille nanométrique et de couches minces nanostructurées.

ACKNOWLEDGMENTS

The undertaking of this project has been a challenging scientific endeavor coupled with a pronounced fulfillment of personal achievement and growth. I would like to express my appreciation to all those who contributed to its conception and completion.

Foremost, to Professor Sylvain Coulombe, my supervisor, for giving me the opportunity to work on such a challenging project, for his moral support, invaluable discussions and guidance. To Professor Jean-Luc Meunier, my co-supervisor, for his timely guidance.

To Helen Campbell – the patient SEM Queen who spent countless hours squinting at grainy images with me.

To Dr Valli and Kelly from Strathcona for their valuable time and discussions around the TEM.

To Florence Paray, Georges Kopps and Dr Ashraf Ismail for liberally bestowing me with time and guidance whenever I would ask for it.

To Frank, Lou and Alain: without their technical expertise, most of us would never make it out of grad school.

A big thank you for the financial support provided by the Natural Sciences and Engineering Research Council of Canada (NSERC), Fonds de recherche sur la nature et les technologies (FQRNT), the Eugenie Ulmer Lamothe (EUL) funds and McGill University.

To my parents, Tariq and Najma, whose unconditional love and support has been the guiding light of my life – thank you for believing in me! To my siblings: Tara, Fahad, Asad and Mohammed – for putting up with my miscellaneous histrionics and to my adorable niece, Maryam Saleha, for providing comic-relief when sorely needed.

To my grizzly, Tuisko, for his friendship, persistent nagging to stop procrastinating and, above everything, his never-ending love.

TABLE OF CONTENTS

LIST OF FIGURES

LIST OF TABLES

THESIS OUTLINE

This thesis is divided into 6 chapters and a concise description of each chapter is as follows.

Chapter 1: Introduction

This chapter opens the thesis with an introduction to the field of study and gives a brief statement of objectives.

Chapter 2: Literature Review

The literature review covers the phenomena and uses of non-thermal plasmas followed by a detailed review of cold plasma systems, process parameters and reactor configurations. A succinct inventory on plasma surface treatment of materials follows. This is continued with a section on the fundamental concepts of plasma polymerization. After which is a section on nanoparticle production techniques. Finally, the techniques are tied together in the remaining sections on nanocomposite thin films and nanoparticle coatings.

Chapter 3: Objectives & Thesis Outline

A definition of the impetus and scope of the dissertation is given followed by a brief outline of the thesis.

Chapter 4: Experimental

In this chapter, the design of apparatus, experimental setup used and its principle of operation and procedures are elaborated on. Furthermore, the analytical methods employed are briefly discussed.

Chapter 5: Results

The results obtained from the characterization of the nanoparticles and films using different procedures are presented in this section (include: OM, FTIR-ATR, TEM and SEM).

Chapter 6: Conclusion, future work and recommendations

The major conclusions arrived upon in this study are summarized in this chapter followed by recommendations for future work to be carried on.

GENERAL INTRODUCTION

Composite materials prepared to have inhomogeniety on a scale smaller than submicron (10^{-7} m) are called nanocomposites. Polymer-based nanocomposites have opened a new horizon of high performance composite materials that find applications in several industrial fields. These compounds incorporate performance-enhancing, nanoscale fillers, which provide properties not otherwise possible with ordinary polymers alone (e.g., bending stiffness, tensile strength, elongation and torque). Improved and unexpected properties such as superconductivity, magnetism, non-linear optics and thermal stability can be achieved owing to enormous interfacial adhesion region characteristics of nanoparticles [1]. Although nanocomposites were first referenced as early as 1950, it wasn't until Toyota Research Laboratories began working with polymer-layered silicate-clay mineral composites in the early 1990s that nanocomposites became more widely studied.

In the past few decades, new processing methodologies have been developed giving rise to hybrid materials containing such morphologies [2] [3]. Several wet processes are currently in use such as: the sol-gel route; *in situ* intercalative polymerization; and *in situ* polymerization. Preparing such materials from randomly dispersed primary particles – methods based on the mixing of polymer and pure, isolated colloids – are not usually successful as the nanoparticles tend to form string aggregates due to their high specific surface energies (typically 500-2000 mJ/m² for inorganic materials [4][5] compared to 20-50 mJ/m² for polymers [6]. The primary particles in such aggregates cannot usually be separated from each other during the processes utilized for nanocomposites creation. As a consequence, nanocomposites with isotropic colloids have been prepared commonly by synthesis of the inorganic particles in situ, for instance in solution, where the solvent can be a monomer and the nanocomposites are then formed by in situ polymerization.

In almost every industry, the nature of a material's surface can drastically affect a product's success. The reasons can be quite different, varying from purely aesthetic to functional. Obtaining the appropriate balance of structural, aesthetic and functional (barrier) properties often requires compounding specific additives into the bulk material or combining several separate materials into a composite structure. A surface treatment is often employed as part of the conversion process to alter the surface characteristics of the specific material being used. Tailoring the surface properties of

materials, via the deposition of a thin film for instance, allows for more flexibility in their uses. Consequently, additional surface modification is implemented in order to achieve the desired properties, while maintaining the characteristics of the bulk material.

One of the most promising techniques for organic thin film production is Plasma Polymerization. The non-thermal plasma polymerization and deposition technique for surface modification, either using a microwave (MW) or a radio frequency (RF) plasma source, has many advantages over the solution-based wet processes. The latter processes constitute of several steps and do not necessarily provide films of satisfactory quality for advanced applications such as microdevices. The reason being that such procedures have little controllability in film microstructure for reasons such as functional polymers having poor solubility; and, moreover, such processes are subject to incorporation of impurities from the solvents utilized [7].

In contrast, the plasma polymerization process is a low temperature, high throughput and environmentally benign one as it is solvent-free. It causes minimal altering to the bulk properties of the substrate, as the extent of modification is usually restricted to the outermost layer [8]. However, such processes are prone to contamination by the incorporation of dust and microparticles. Such impurities, when introduced in the films in an uncontrolled manner, cause performance degradation and early failures [9]. Consequently, special care must be taken in order to control such contamination.

Lately, the concept of controlled incorporation of nanometric-sized particles into thin films has grown in attention due to the extraordinary properties of nanocomposites thin films [10]. Conversely, nanometric-sized particles are exceptionally challenging to handle outside processing reactors due to their tendency to form agglomerates. Therefore, an integrated process of particle fabrication, transport and pre-coating in a non-thermal plasma, followed by co-deposition in a polymer matrix layer will be developed in the present thesis as a route to nanocomposites thin film production. Furthermore, an attempt will be made to co-deposit fullerene (C_{60}) nanoparticles into a matrix of plasma-polymerized polyethylene as a validation test for the newly developed system.

2.1 PLASMAS

Plasmas, also referred to as the fourth state of matter, may be broadly defined as a quasineutral gas that exhibits a *collective* behaviour in the presence of applied electromagnetic fields. Plasmas are partially ionized gases comprising of electrons, ions, radicals and neutral atomic and molecular species. This definition is broad enough to encompass the spectrum of space and man-made plasmas extending from the sun, stars, solar winds and the aurora borealis to the regime of plasma spraying torches, fusion reactors, fluorescent tubes and mercury-arc lamps.

Plasmas are currently widely employed in industry and their range of application broadens continuously. The usefulness of plasmas in technology can be ascribed in two qualities: plasmas make accessible much higher temperatures than those that could be achieved by conventional methods such as chemical fuel torches. This allows for their use in the treatment of toxic wastes (e.g. batteries, hospital and aeronautical). Also, a large variety of reactive species (excited atoms, ions and radicals) are generated within the plasma, allowing for new material synthesis (e.g. C_{60}, CNT and diamond films) [11].

The energy required for the generation of a plasma can have varying sources. By far, the most frequently employed route for plasma generation is via the application of electromagnetic fields to a gas. Primarily, energy is introduced into the plasma by the acceleration of electrons in a DC, RF or microwave field. These electrons then fragment, excite and ionize particles by inelastic collisions. In processing plasmas, the volume density of the various gaseous species, their energies and numerous other properties depend on a number of factors including: mode of plasma generation, processing parameters (e.g. gas flow rate, operating pressure and power input), and the system geometry (e.g. electrode configuration).

2.2 PLASMA GENERATION

Plasma processes are being used in a myriad of applications in industries dealing with products as varied as medical disposables and prosthetic devices to high voltage coils, electronic housings and painted fascias. The most typical configurations for plasma generation are: *(i)* DC diode discharge; *(ii)* RF (radio frequency) discharge; *(iii)* Magnetron enhanced discharge; *(iv)* Microwave discharge; *(v)* Vacuum arcs, and; *(vi)* Plasma arcs [12]. Figure 2.1 shows a schematic of some of these plasma generation configurations.

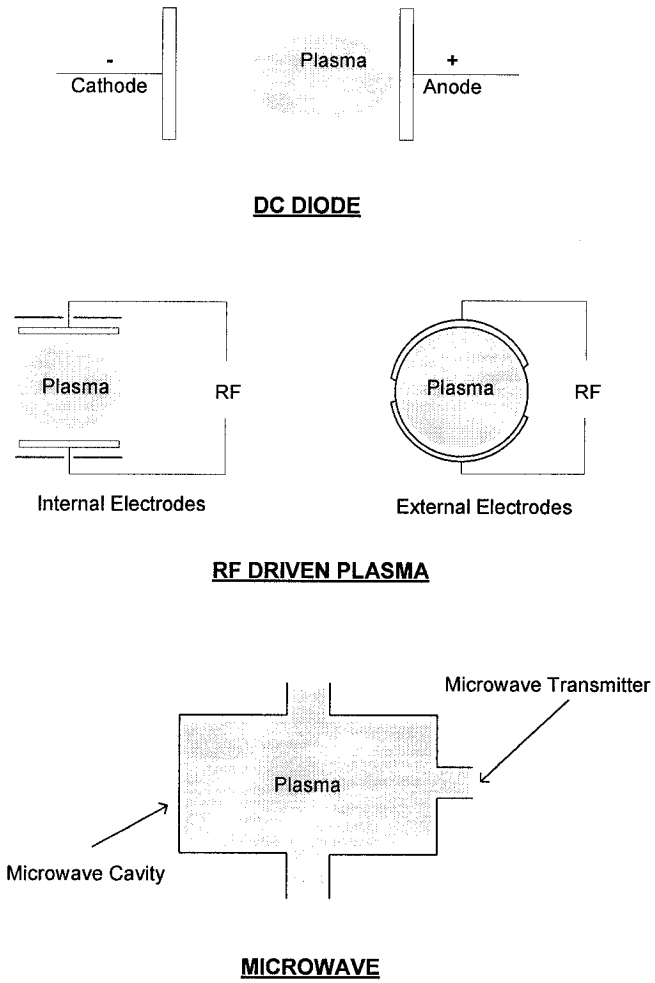

Figure 2.1: Miscellaneous plasma generation configurations

The simplest method for plasma generation uses the action of an electromagnetic field on a gas to produce electrical breakdown of the medium. The external field can be supplied by DC *electrical power*, in which electrodes must collect real currents of impinging ions or electrons, or RF *excitation*, in which the power is coupled to the plasma by displacement currents, without a requirement that real current flows to the electrodes. The absence of real current removes a potential source of sputtering and consequent plasma contamination [13]. This is a major factor in the dominance of *electrodeless* RF plasma sources for microelectronics and surface treatment applications. The advantages of RF discharges over the DC discharges, as summarized next, explain the wider spread in industry of RF plasmas as compared to DC plasmas:

1. RF plasmas can be excited and sustained using either conductive or nonconductive electrodes, while DC discharges require the electrodes to be conductive throughout the process

2. RF plasmas can be sustained with internal as well as external electrodes while DC discharges require the electrodes to be inserted inside the reactor and be in direct contact with the plasma. Use of external electrodes is sometimes required when the gases of the discharge are corrosive or when one wants to reduce contamination of the plasma with the material of the electrodes

3. RF plasmas are characterized by higher ionization efficiencies than are the DC plasmas

4. RF plasmas can be sustained at lower gas pressures than DC plasmas

5. In RF plasmas, the energy of the ions bombarding the sample is controlled by the negative bias, which can be adjusted over a wide range of values. Samples placed on the cathode of the DC discharge are exposed to bombardment of high energy ions that are accelerated at voltages that have to be above the minimal breakdown

voltage which is not readily controllable and is inherent to the system. This can cause damage to sensitive substrates

2.3 PLASMA CLASSIFICATION

The plasma state exists in natural form in the cosmos or is created under unique conditions for specific purposes. The plasmas found in nature cover a large range of electron densities and temperatures[1], as shown in figure 2.2.

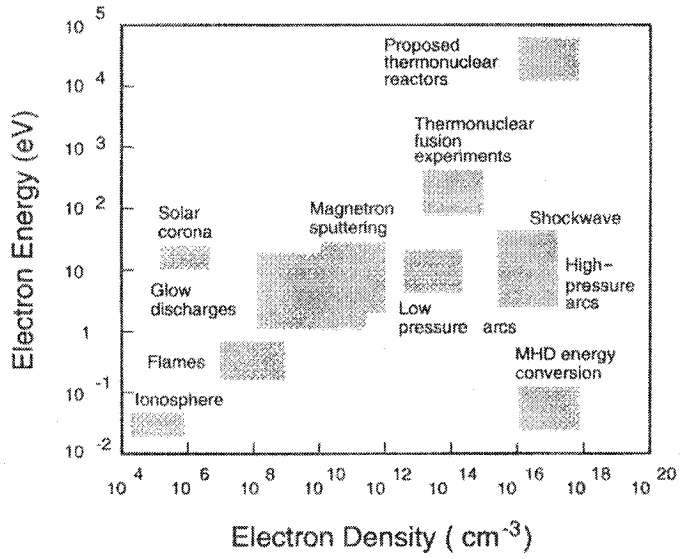

Figure 2.2: Plasma types by electron density and temperature/energy [14]

Taking into account the wide range of parameters, the plasmas are classified into several categories, succinctly listed as follows:

- Plasmas in *complete thermodynamic equilibrium – CTE plasmas*. In a CTE plasma, all temperatures are equal [T_g *(temp. of gas)* = T_{ex} *(excitation temp.)* = T_{ion} *(ionization temp.)* = T_d *(dissociation temp.)* = T_r *(radiation temp.)* = T_e *(electron temp.)*]. Such conditions imply that photons and other particles are in collisional-equilibrium and consequently, no radiation (photon) leaves the plasma volume. CTE plasmas exist only in stars or during the short interval of a strong

[1] 1 eV = 1.6022 x 10^{-19} J. This corresponds to a Maxwellian electron gas at 11,600 K

explosion. They have no practical importance because they do not exist in controlled laboratory conditions.

- Plasmas in *local thermodynamic equilibrium – LTE plasmas*. These are plasmas in which all temperatures, except T_r, are equal in each point within the plasma. They are characterized by a significant emission of radiation and are referred to as *thermal plasmas*.

- Plasmas that are not in *local thermodynamic equilibrium – non-LTE plasmas*. These plasmas are characterized by different temperatures for the electron and heavy particle gases. They are also commonly referred to as *cold plasmas / non-thermal plasmas*.

The plasmas produced for research or manufacturing purposes are either LTE or non-LTE type plasmas, designated in daily use, respectively, as thermal and non-thermal plasmas.

2.3.1 THERMAL PLASMAS

LTE plasmas can generally exist under two conditions [15]:

(i) When the heavy particles are very energetic, at temperatures of the order of 10^6 - 10^8 K (10^2 - 10^4 eV)

(ii) When the pressure is atmospheric, even at temperatures as low as 6,000 K

An increase of pressure in the plasma causes an increase in the frequency of inter-particle collisions, thereby enhancing energy transfers and thus leading to the thermalization of the electrons with the heavy particles. Consequently, when the pressure in the system increases towards atmospheric pressure, the two systems tend to reach the same thermodynamic equilibrium temperature, as shown in figure 2.3 for a DC discharge [16].

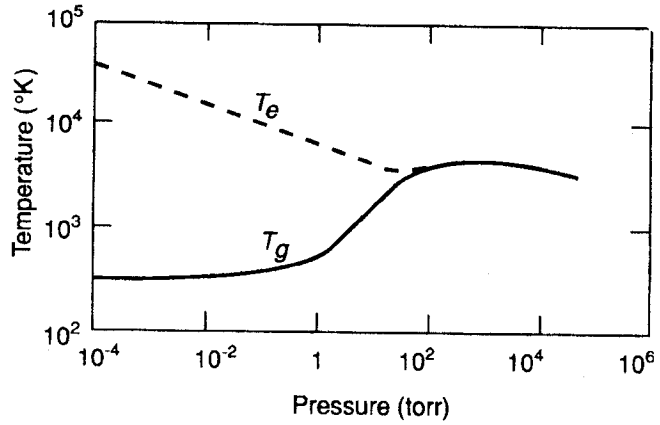

Figure 2.3: Electron and ion temperatures as a function of pressure

Such LTE plasmas at atmospheric pressure are called *thermal plasmas*. This relatively high temperature medium (~10,000 – 30,000 K, typically) which can be maintained in a modest volume tends to be suitable for applications requiring high specific enthalpies. Some typical applications of thermal plasmas are in the generation of refractory coatings by plasma spraying processes and in extractive metallurgy, for reduction, or for smelting of ores.

2.3.2 NON-THERMAL PLASMAS

As mentioned before, in low-pressure discharges / non-LTE plasmas, thermodynamic equilibrium is not reached, even at a local scale, between electrons and the heavy particles. In non-LTE plasmas, the temperature of the electrons can be much higher than that of the heavy particles and $T_e >> T_i > T_g$. The electrons can reach temperatures of 10^4 – 10^5 K (1-10 eV), while the temperature of the gas, T_g, can be as low as room temperature. As the heavy particles are mostly responsible for the thermal energy transfers, such plasmas are referred to as *cold plasmas*.

The cold plasmas have been developed specifically and purposefully based on their nonequilibrium properties and their capability to cause physical and chemical reactions

with the gas at relatively low temperatures. Applications of cold plasmas are widespread and put to use in a variety of fields, from microelectronic fabrication to surface hardening of metals. Energy input by non-thermal means is a powerful and wisely used process tool in thin-film production processes. In thin-film deposition, most of the energy enhanced techniques involve the use of a plasma. The main feature of the plasma state utilized for material treatment is a non-thermodynamic equilibrium condition, i.e. the system is not defined at all thermodynamic states by one temperature [17].

Most of today's non-thermal plasma sources operate at reduced pressures ranging around $1\text{-}10^4$ Pa [13]. Here, the mean free path of the particles is much larger than in high-pressure thermal-systems. Therefore, the primary viable route for energy transfer in the system is via electron collision processes. This is attributable to the fact that electrons, being the lightest and fastest moving particles in the plasma medium, acquire energy more readily from the external electromagnetic field than the heavier species. This is then redistributed to the remaining species via the abovementioned collision process. Consequently, energy transfer is made significantly insufficient due to the reduced number of collisions and sizeable mass differences between the colliding pairs.

Macroscopically viewed, the system remains at ambient temperature while containing electrons that retain most of the energy they acquire from the accelerating field. This results in high electron temperatures - T_e – which can be well above 10,000 °C. A fairly good fraction of this energy is channeled into the creation of neutral excitations and fragmentations into atoms and radicals via inelastic electron-particle collisions allowing for chemical specificity in non-thermal plasmas. For these reasons, glow discharges are cold systems with a large number of atoms and radicals which can be regarded as species active for treatment processes and for the formation of films. Therefore, they can be used for surface treatment processes such as etching and deposition without producing thermal degradation, even for plastic substrates. A schematic summary of the different types of reactions that can take place in a cold plasma reactor are illustrated in figure 2.4.

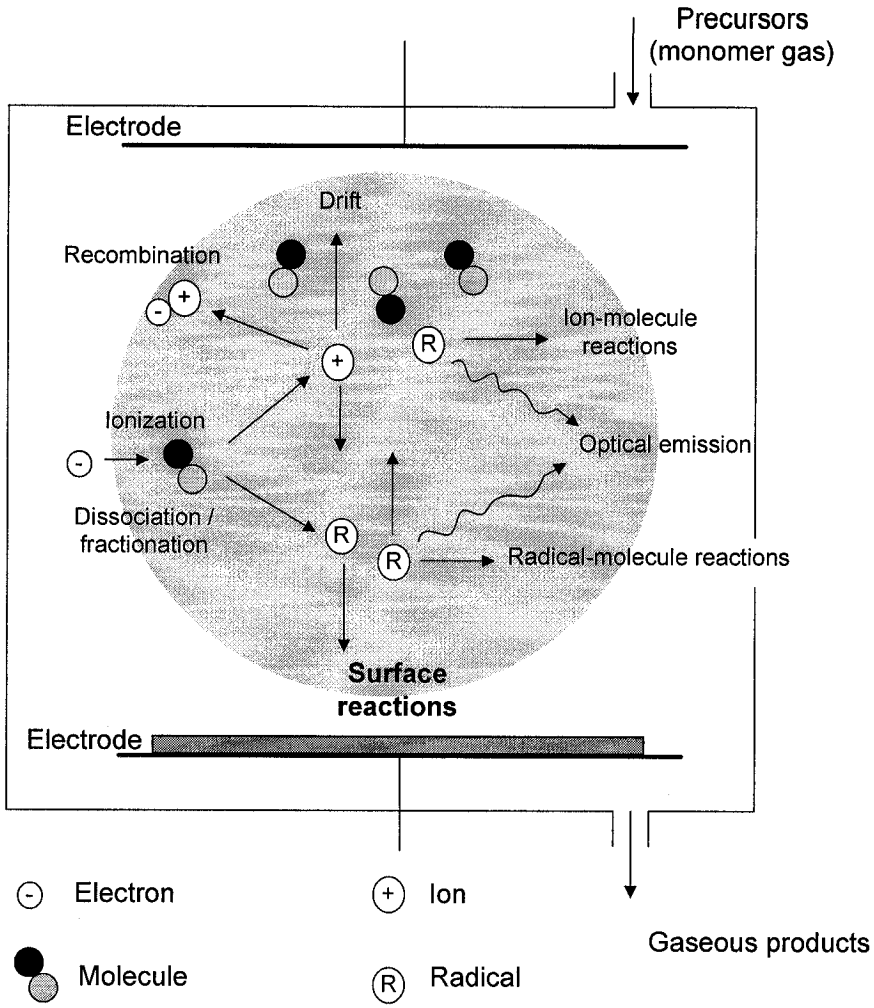

Figure 2.4: Schematic diagram of reactions in a plasma reactor

2.4.1 COLD PLASMA SYSTEMS

A block diagram of a cold plasma system used for material processing is shown in figure 2.5. Generally, it consists of several subsystems providing different necessary functions which are described below.

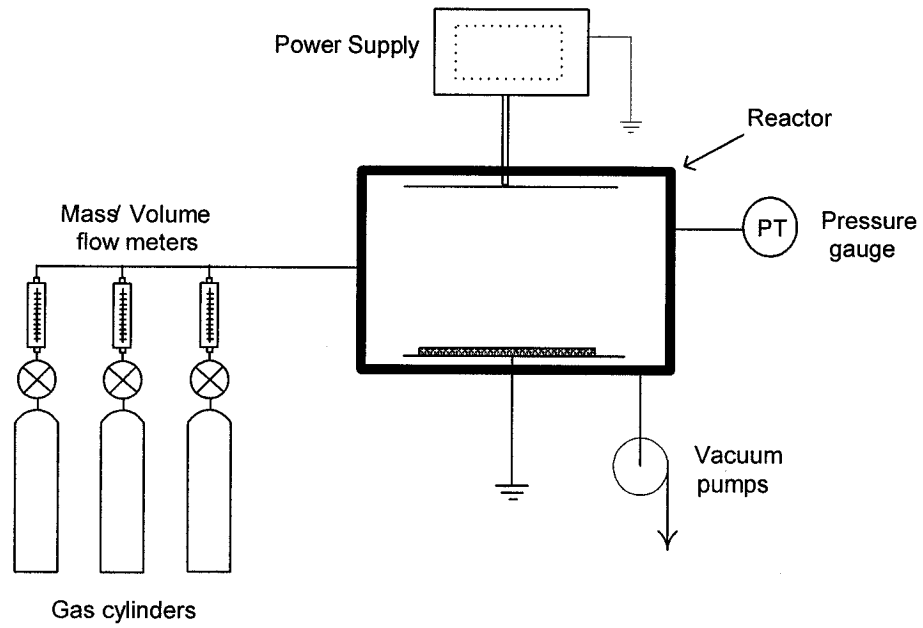

Figure 2.5: General outline of a system for cold plasma processing

1. *Gas handling system.* This includes:
    a. *Precursor gas supply.* The source materials or precursors are in most cases gases in high-pressure cylinders or liquids with sufficiently high vapour pressures. Solids with reasonable vapour pressures are also used as precursors sometimes.
    b. *Mass / Volume flow controllers.* These are used to measure and control the flow of different gases fed to the reactor.
    c. *Vacuum system* (comprising of pumps and pressure controller). The plasma reactors for materials processing operate at pressures between 10^{-4} and ~ 10 torr. However, lower background pressure is often required to ensure cleanliness of the process. Therefore, the whole range of vacuum pumps, from mechanical to cryogenic, are used; the types and sizes of the pumps are determined by the required vacuum levels and gas flow rates.
2. *Plasma Reactor.* This includes a chamber within which a plasma is ignited. This is made of materials such as quartz and stainless steel (contingent on the application) and can have a wide range of auxiliary equipment such as electrodes and substrate holders.
3. *Power supplies.* The role of power supplies is twofold: to sustain the plasma in the

reactor and to provide a controlled external substrate bias when required for certain processes.

4. *Safety devices* for handling hazardous gases. Most precursors used in plasma processing are hazardous and toxic (corrosive, highly toxic, flammable or explosive). Some of the safety devices required when dealing with such hazardous materials are:
    a. *Flow limiters*, mounted between the valve of the supply cylinder and the pressure regulator to prevent excessive flow of the gas in case of breakdown of pressure regulator.
    b. *Flashback arresters*, required when using flammable or explosive gases to prevent fire propagation to the gas in the cylinder.
    c. *Fumehoods, scrubbers and/or diluters*. These are used in order to accommodate the exhaust from pumps.

2.4.2 PROCESS PARAMETERS

For a given system, the outcome of the process is strongly dependent on its operating parameters. A comprehensive list of the process parameters that can affect the end result of plasma processing is given in table 2.1.

Table 2.1: Parameters controlling materials processing by cold plasmas [18]

Plasma Processing Parameters		
Kinetic (gas system)	Electrical (plasma system)	Surface (substrate system)
Precursor gases	Frequency (DC to GHz)	Material
Carrier gases	Free fall	Conducting
Mass/Volume flow rates	Mobility	Insulating
Pressure	Diffusion	Temperature
Gas delivery location	Electrode geometry	Position
	Electrodeless	
	Electrode	
	Discharge power	
	Field strength	
	Current density	
	Particle energy	
	Active neutrals	
	VIS to UV radiation	
	Electrode material	

The classification of these parameters largely complies with the first three subsystems described before. The following list names the most important parameters among those in table 2.1.

- Partial pressures of the feed gases, or flow rates of the different feed gases
- Total pressure in the reactor
- Substrate temperature and bias
- Reactor geometry and material
- Electrode material and distance between electrodes
- Electric power applied to the plasma

These parameters have to be carefully controlled to define the plasma chemistry and to achieve the desired results. The relationship between the macroscopic variables of a cold plasma processing system and the microscopic plasma parameters is complex and is appropriately illustrated in figure 2.6. Changes in macroscopic plasma variables such as composition of feed gas, flow rates, pumping speed, electrical discharge power, and frequency will generally change the basic plasma conditions. However, the precise manner of these changes is, in most cases, unknown.

The RF power determines the current and voltage between the electrodes. The composition of the gas mixture can effect the chemical reactions inside the plasma reactor and the properties of the final product, for example: the composition of deposited film or the anisotropy and selectivity of etching. The composition of the feed gas, the total pressure in the reactor, and the electrical power will each affect the rates of the reactions. These can be affected by the distance between electrodes and the substrate bias or temperature as well. The last two plasma parameters can also affect the structure of a deposited film or the etching anisotropy. The flow rates, total pressure, and reactor geometry can determine the uniformity of the process.

The gas flow rate, the pumping speed and the pressure are interrelated. The pressure can be changed in two ways: by changing the flow rate at a constant pumping speed or by changing the pumping speed at constant flow rate. While the two methods can provide the same pressure, they result in different residence times for the species in the reactor and that can cause changes in the chemistry of the process [19].

The frequency of the electric field is also a system parameter that can affect the plasma process or the properties of the product. A variation of the frequency can affect the number and energy of ions that can follow the alternating field, thus changing the flux and energy of the particles bombarding the plasma treated surface. Lastly, the building materials of the reactors and electrodes are an important factor to be considered as the

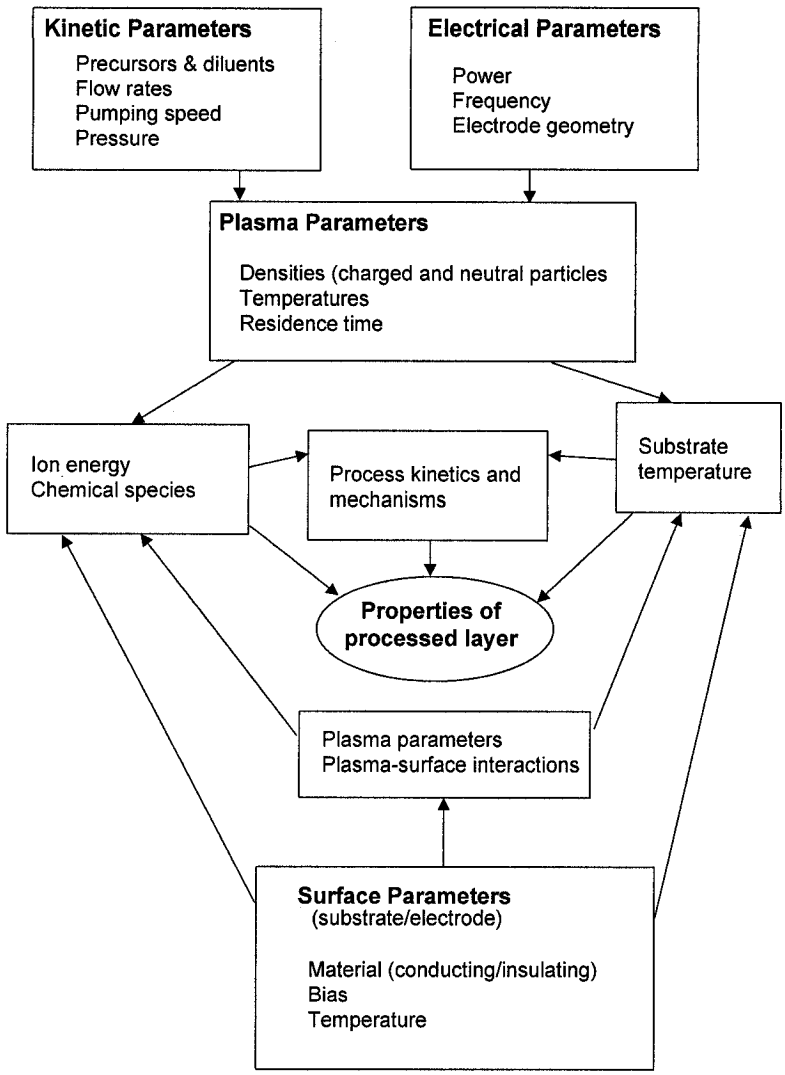

Figure 2.6: Complexity of interaction between plasma variables [20]. The arrows indicate the possible interactions between process parameters; they do not indicate that all the described interactions always take place

material used can change the chemistry occurring in glow discharges. The materials should be chemically inert to the precursor gases and to the plasma products. Since surfaces immersed in a plasma always adopt a negative potential relative to it, the electrodes and reactor walls will almost always be sputtered to a certain degree. These sputtered atoms may contaminate the plasma and the processed samples or, they could be incorporated in a deposited film. Such possible effects should be taken into consideration when designing a reactor and, furthermore, process parameters must be precisely controlled to achieve the required results and process uniformity.

2.5 RF REACTORS

The power supplies used to sustain commercial RF plasma systems are operated at specific frequencies established by international agreements [21]. The most used frequency is 13.56 MHz and sometimes, the higher harmonics of 27.12 MHz and 40.68 MHz are also utilized. The RF generators are designed to operate at a constant output impedance of 50 Ω. However, the impedance of the glow discharge under RF excitation is generally much higher and contains a complex component associated with its capacitive and/or inductive nature; $Z=R+jX$, where R, the real part of the impedance is the resistive component while X, is the reactance of Z ($j = \sqrt{-1}$). As a consequence, in typical applications, only 20-40% of the input power is available as plasma enthalpy without a matching network [22]. An impedance matching network/unit is thus required between the RF power supply and the reactor as, otherwise, most of the power will reflect to the power supply instead of being absorbed into the plasma. When properly tuned, the matching unit compensates for the reactive impedance such that the power supply sees a purely resistive load ($X=0$).

When using high-frequency power supplies, it is possible to transfer energy to the plasma without inserting the electrodes inside the reactor – if a suitable coupling between the power supply and the reactor is used. For such a design, the reactor is usually built from dielectric materials such as quartz or Pyrex. Since the electrodes are not in direct contact with the discharge, the plasma formed is called an *electrodeless discharge*. Electrode designs for transferring the power to the plasma in electrodeless discharges are illustrated in figure 2.7.

These electrodes correspond to two types of coupling of the RF power to the electrodeless plasma and it is elaborated on as follows:

1. *Inductive coupling*, in which a coil is connected to the power supply through a matching unit and is in turn, wound around a tubular reactor (as shown in figure 2.7 (a)).

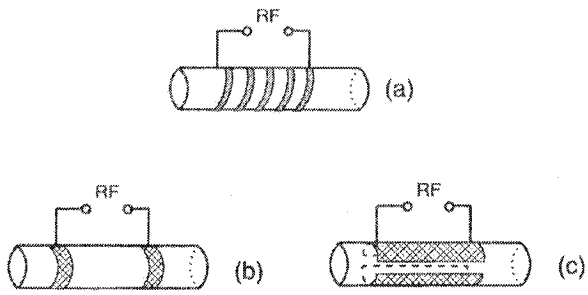

Figure 2.7: RF coupling methods to electrodeless reactors

2. *Capacitive coupling*, in which the RF power is transferred between two separated electrodes mounted outside the reactor. The electrodes can be shaped as two rings mounted around the reactor as shown in figure 2.7 (b) or two parallel plates placed along the reactor, as shown in figure 2.7 (c). This configuration also requires a matching network as stated previously.

Although the terms *inductive* and *capacitive* are often used as just defined, the inductive coupling is not purely inductive and has an accompanying capacitive component to it through the walls of the reactor. In fact, we say that the system is inductive when the overall load reactance $X > 0$, and capacitive when $X < 0$. Thus, when an inductive coupling is used, deposition on the walls is often observed to follow a pattern matching the shape of the coil. This is an indication of localized stronger electric fields on the walls consequently showing that the coupling is at least partly capacitive through the walls of the reactor [18].

In a tubular reactor of the types shown in figure 2.7, and especially in figure 2.7 (a), the strength of the electric field is not uniform along the reactor. Therefore, the substrate position inside the reactor becomes a parameter that can affect the result of the process and can be controlled to achieve desirable properties [23], [24]. In tubular reactors, the substrates are usually positioned with their surfaces perpendicular to the axis of the reactor. These types of RF reactors are also referred to as *barrel reactors* and are used,

sometimes, for industrial applications, although they are more popular in research laboratories, being relatively inexpensive and easy to set up.

2.6.1 PLASMA SURFACE TREATMENTS

Research and development for new, improved materials and their manufacturing processes have been rapidly accelerating during the last decades. This multi- and interdisciplinary effort encompasses many fields of science and technology such as physics, chemistry and materials and chemical engineering. One of these rapidly-growing areas is processing by plasma assisted methods. A search of published literature over the past 35 years shows an enormous growth in plasma assisted research and development activities, which reflects the significant task undertaken to understand these processes and use them in novel applications or as a useful substitute to established techniques.

The use of cold plasmas for materials processing has gained acceptance in a large number of technologies, from metallurgy to manufacturing of computer chips, and covers a wide variety of materials, including metals, semiconductors and polymers. Most applications of plasma enhanced chemical processing focus on treating solid surfaces, film deposition, modification of surfaces and etching of surface layers. Cold plasmas are also used to synthesize gases or liquids as final products.

Plasma enhanced chemical processing (PECP) takes advantage of the high-energy electrons present in glow discharge to dissociate and ionize the molecules of the gas to form chemically reactive radicals and ions. Since such conditions do not require the need of thermal energy for bond breakage/dissociation, reactions can be promoted at low temperatures (< 200 °C). These relatively low temperatures provide one the primary benefits of processing with cold plasmas. With PECP, it is possible to process substrates that do not have the thermal stability necessary to withstand processing at higher temperatures. Low processing temperatures may be imposed by the substrate of the nature of the film being deposited (e.g. polymer). Low temperatures may also be

required to preserve properties achieved by prior processes, for example, heat treated metals. In addition, treatment at lower temperatures possible in the plasma is critical when one has to limit diffusion, or grain growth, especially in microelectronics where very small feature sizes and shallow junctions are involved.

All plasma enhanced chemical processes are the result of chemical reactions, the main difference between the various processes being the state of the final product. For deposition of films, the product of the reactions has to be nonvolatile and also be able to deposit on the substrate. In some surface modification applications, such as nitriding and oxidation, the gas is dissociated in the plasma, forming radicals that react with the surface to form a nonvolatile product that remains on the surface and changes the characteristics of the surface layers. For cleaning, ashing or etching, the products of the reaction between the plasma species and the substrate have to be volatile to remove material from the exposed surface.

Cold plasmas can deliver a uniform flux of energetic particles (e.g., positive ions, neutrals, metastable species, electrons and photons) whose energy and flux can be controlled. The substrates are therefore subjected to bombardment with energetic particles, which impart both physical and chemical components to the plasma treated surfaces. The bombardment of the surface by the ions accelerated through the plasma sheath can affect the processes occurring at the surface and the properties of the processed surface or deposited film. The physical component can induce directionality during film etching, or, it can alter the properties of the deposited film by promoting surface reaction steps. The combination of physical processes with purely chemical reactions yields process rates and material properties unattainable with either process separately.

The use of plasma processing has been expanded due to the necessity to avoid problems associated with the disposal of chemicals used in alternative wet processing techniques. A summary of applications of cold plasmas is presented in table 2.2. The applications are

classified according to the type of feed gas, the product of surface reactions and the intensity of ion bombardment.

Table 2.2: Classification of plasma applications [25]

		Reactive Gas Plasma	
	Inert Gas Plasmas	Nonvolatile Surface Product	Volatile Surface Product
Low ion bombardment	Plasma cleaning	Plasma oxidation, surface activation, surface hardening, polymerization, film deposition	Surface activation, plasma ashing, plasma etching
High ion bombardment (high negative bias)	Sputtering, sputter etching	Reactive sputter etching	Reactive ion etching

Over the years, several methods have been developed to modify material surfaces for improved interface characteristics. These include mechanical treatments (e.g. roughening by abrasion), wet-chemical treatments with strong acids and bases, and exposure to flames. However, the most versatile, reproducible and environmentally affable methods involve plasmas. A vital feature of plasma techniques is that the surface properties of the treated materials can be modified without changing their intrinsic bulk properties. Tailoring of materials for multifaceted applications is an expanding field, whereby, most often, the surface properties must be adjusted. Consequently, surface coating by thin films is a promising way to modify the surface properties.

Organic thin films have received a great deal of interest due to their extensive applications in the field of mechanics, electronics and optics. Applications include chemical, physical and biological sensors, microelectronic, non-linear optical and molecular devices. In spite of the large number of studies conducted in this area, only a few cases have been reported of the successful implementation of these materials for electronic and optic-based applications. This is largely due to the fact that organic thin

films often show poor thermal and chemical stabilities and poor mechanical toughness [26].

Therefore, it is of interest to develop polymer thin films of high quality for a variety of industrial applications. A variety of techniques for producing polymer thin films have been studied. Ultrathin polymer films can be prepared in two ways: one includes wet processes like Langmuir-Blodgett, spreading, dripping or solvent casting methods; the other is dry processing, such as physical and chemical vapour deposition (PVD and CVD respectively). Of these methods, the CVD methods, such a plasma polymerization, are frequently employed to make polymer thin films [27]. Plasma enhanced chemical vapour deposition (PECVD) is an excellent alternative to depositing a variety of thin films at temperatures lower than those utilized in CVD reactors. This is attributable to the nature of plasma that functions, amongst other things, as: a catalyzer for an ongoing CVD process and/or; initiating one that would not occur under purely CVD conditions.

Plasma synthesized thin films have been receiving much interest in recent years because of their excellent properties. Plasma treatment of metal surfaces and deposition of coatings by plasma polymerization can be carried out in a variety of coupling modes of electromagnetic energy to gas and/or monomer vapour. Plasma polymerization can be shown to be a superior technique for forming polymer thin films thinner than 100 nm from almost all organic vapours without the necessity of having functional groups normally associated with conventional polymerization [28]. It is a one-step process, replacing the several functional steps employed in wet-polymerization.

The thin films fabricated via this technique have various advantageous characteristics such as flawless thin coating, good adhesion to substrate surfaces, mechanical toughness and thermal stability. This leads to a wide variety of potential applications (e.g. perm-selective membranes, protective coatings and electrical films). This method of synthesis has become instrumental in fabricating semiconductor devices and further efforts have been made to apply these films to other fields such as optical devices, separation films and biomedical materials.

2.6.2 PLASMA POLYMERIZATION

Plasma polymerization (PP) is a new material preparation *process* and is not a kind of polymerization. The materials formed by PP are vastly different from conventional polymers and constitute a new kind of material. PP has been dealt with, however, as an extension of polymerization from the academic viewpoint and as a new technology to prepare thin films from a practical viewpoint.

PP covers a wide interdisciplinary area of physics, chemistry, interfaces, materials, and so on. It is essentially a PECVD process resulting in the deposition of an organic polymer. It refers to the deposition of polymer films through plasma dissociation and excitation of an organic monomer gas, and subsequent deposition and polymerization of the excited species on the surface of the substrate. PP is used to deposit films with thicknesses from several tens to thousands of angstroms and the deposited films are called *plasma polymers*. These are generally chemically and physically different from conventional polymers and are also different from most inorganic materials [29].

PP is a strongly system-dependent process whereas conventional polymerization is based on molecular processes during which rearrangements of the atoms within the monomer seldom occur. In contrast to such molecular processes, polymer formation in a plasma is an atomic process. Polymers formed by plasma polymerization are, in most cases, highly branched and cross-linked. Free radicals formed on the surface of polymers and other solid materials exposed to a plasma can be used to initiate graft polymerization. PP is characterized by several features [28], [29].

1- Plasma polymers have no discernible repeating units as do conventional polymers.
2- The properties of the plasma polymer are determined by plasmas parameters and not by the monomer used. Case example: there is no single product which can be identified as the plasma polymer of ethylene since a variety of products can be

obtained from an ethylene plasma; plasma polymers of ethylene are not polyethylene.

3- The monomer used for plasma polymerization does not have to contain a functional group (such as a double bond), for PP to take place.

PP can be used to prepare a variety of products including: oils; powders; soluble polymers; and insoluble films. The plasmas utilized for the plasma deposition of polymers can be categorized according to precursors utilized to being: non-polymer-forming plasmas and; polymer-forming plasmas. In the former category, the feed gases used are nonpolymerizable (e.g: N_2, H_2, NH_3). In the latter category, the feed gas, or monomer, is polymerizable in the plasma in the sense that itself, or parts of it, can be used as the building blocks of macromolecules. Plasmas of methane and styrene are considered to be polymer-forming plasmas, although methane can not be polymerized by conventional methods [28]. Almost all organic compounds that have sufficient vapour pressure to be fed into a plasma are polymerizable. Monomers used for plasma PP include hydrocarbons, fluorocarbons, sulfides, siloxanes, silanes and so on.

PP takes place through several reaction steps – initiation, propagation, termination and reinitiation [31]. In the initiation stage, free radicals and atoms are produced either by collision of energetic electrons and ions with monomer molecules or by dissociation of monomers absorbed on the surfaces exposed to the plasma. The propagation of the reactions, being the formation of the polymeric chain, can take place both in the gas phase and on the deposited polymer film. In the gas phase, propagation involves the addition of a radical atom to another radical or molecule. At the surface of the polymer film, propagation occurs through interactions of surface free radicals with either gas phase or adsorbed monomers. Termination also takes place either in the gas phase or at the polymer surface by processes similar to the propagation step but ending either with the final product or a closed polymer chain.

In conventional polymerization, the termination step interrupts the process, whereas in PP, the neutral products formed in the termination step can undergo reinitiation and

propagation reactions. In the reinitiation processes, chain fragments can be converted into radicals by collision with electrons in the gas phase or by impact of energetic particles or via photon absorption on the surface of the polymer film.

The described homogeneous polymerization in the plasma phase and the heterogeneous polymerization at the surface of the growing film can be summarized by the reaction scheme proposed by Poll et al. [32] and illustrated in figure 2.8.

As shown in this figure, the gaseous precursor monomers can: polymerize in the plasma and deposit as a film (reaction path 1, characterized by a rate k_1); be converted in the plasma into reactive products (path 2); or be converted in to nonreactive products (path 4). The reactive products can convert into depositing a polymer film (path 3) or be converted to nonreactive products (path 5). Degradation of the formed polymer film can occur from nonreactive products (path 6).

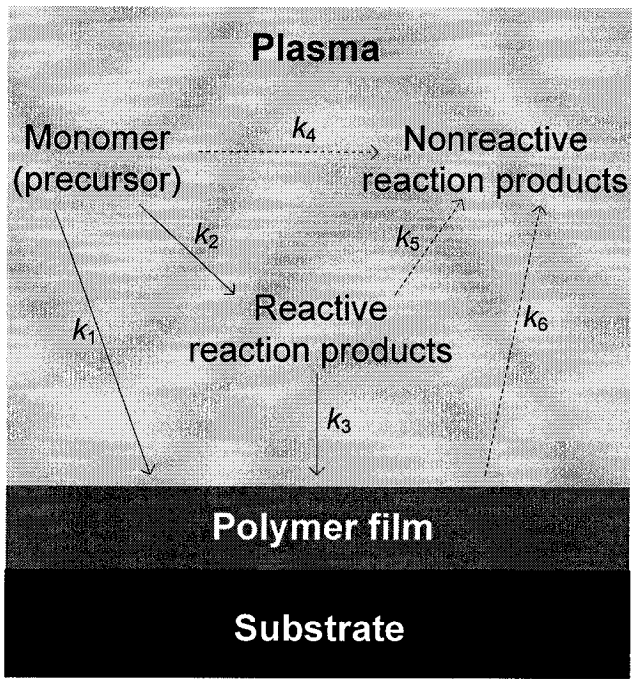

Figure 2.8: Diagram of plasma polymerization. Solid line: polymer deposition path; broken line: volatile product formation line

Path 1, by which the monomer is directly polymerized into a growing film, is also called *plasma induced polymerization*. This is essentially a conventional molecular

polymerization process, triggered in this case by reactive plasma species. Plasma induced polymerization can take place only if the original monomer contains polymerizable functional groups, such as double, triple, or cyclic bonds [33].

Deposition of a polymer film through paths 2 and 3 is *plasma polymerization*, where the intermediate reactive products can be ions, excited molecules, and free radicals not necessarily preserving the original monomer [33]. The monomer does not need to have polymerizable groups in order to undergo PP. Compounds such as tetramethylesilane (TMS) or tetramethyltin (TMT) are nonfunctional and therefore do not polymerize via conventional polymerization. In a plasma, the sylmethyl and tinmethyl units dissociated by electron impact become functional groups and can then polymerize. Ethane and methane can be polymerized in a plasma and using unsaturated fluorocarbon gases, such as tetrafluoroethylene, Teflon®-like films can be deposited.

Unlike conventional organic polymers, plasma polymers do not consist of chains with regular repeated units but tend to form an irregular 3-D cross-linked network. Surface treatment by PP has been used in interface engineering for improving adhesion, hydrophobicity, hydrophilicity, printability, corrosion resistance and selectivity of material surfaces. PP films have several advantages over conventional polymers in the synthetic process; some of which are listed as follows [34]:

1) The starting feed gases used do not have to contain the type of functional groups normally associated with conventional polymerizations

2) The entire process is truncated into one-step as opposed to several steps encountered via conventional polymerization routes

3) Films are often highly coherent and adherent to a variety of substrates, including polymers, glasses and metals

4) Polymerization is carried out without the use of solvents, thus making the procedure environmentally amicable

5) With careful control of the polymerization parameters, it is possible to produce chemically functionalized surfaces along with other chemical and physical film surface characteristics

Several excellent review articles exist pertaining the advances in polymer this film deposition via PP [35], [36], [37].

2.6.3 PLASMA POLYMERIZATION PARAMETERS

The most distinguished characteristic of plasma polymerization is that the chemical structure of plasma polymers obtained from the same monomer is not unique and is largely controlled by reaction parameters. The plasma parameter that appears to control the deposition of polymer films under constant conditions of pressure, plasma excitation energy, and monomer is the power (*W*) to flow-rate (*F*) ratio (*W/F*) [38]. This parameter reflects the n_e (electron density), which increases with increasing power, and residence time which in turn increases with F^{-1}.

A modified parameter, which takes into consideration the molecular weight of the monomer, *M*, is *W/(FM)* [30], [39]. This parameter indicates the energy input per unit mass of monomer. For homologous monomers in similar reactors, the behaviour of the process parameters as a function of *W/(FM)* is generally not affected by the molecular weight of the monomer. The chemical structure of plasma polymers is controlled by the fragmentation pattern of the monomer in the plasma. As the dissociation of a monomer into reactive fragments in the plasma is to be related to the specific energy received per unit molecule, *W/(FM)*, the control of the chemical structure by this parameter is well rationalized and it has been shown that the chemical structure of a plasma polymer obtained at a specific value of *W/(FM)* was unique for different choices of individual *W* and *FM* [40].

The range of structure control by *W/(FM)* extends over two completely different types of materials that are distinguished from each other in their basic chemical structures:

- Polymers which are composed of linear covalently bonded monomers
- Inorganic materials which are composed of three-dimensional tight covalent networks

At relatively low values of *W/(FM)*, a plasma polymer is obtained whose structure and properties are very similar to those of a conventional polymer. On increasing the parameter value, the chemical structure changes gradually to a more dense covalent

network with less organic groups, such as CH_3 or CH_2, until it is almost completely composed of tetrahedrally bonded inorganic structures at extremely high values of *W/(FM)*. Most plasma polymers, which are distinguished from conventional polymers, consist of a structure that lies somewhere between the polymeric and inorganic materials and are in the form of a highly cross-linked and three-dimensional network [30].

2.7 FULLERENES

The material used in this project as a filler for the composite films and for nanocoating experiments is fullerenes, C_{60}. The discovery of carbon cage molecules, C2n (or *fullerenes*), by Smalley, Kroto and coworkers in 1985, launched an intensive interdisciplinary inquiry into the fundamental properties of these highly symmetrical molecules. The subsequent observation by Kratschmer, Huffman and coworkers that C_{60} and C_{70} could be produced in large quantities to be studied in the solid state opened up this research area to physicists, chemists and materials scientists, and the field of fullerene-based materials was born. In addition to the interesting chemical, physical and photophysical properties of the isolated molecules, many exciting material properties were discovered when they were assembled in solid state.

Fullerenes are cage-like all-carbon molecules which under special circumstances, such as high intensity photon or electron irradiation, ion plasma excitation, pressure, or doping, may form polymeric solids. Fullerenes are also used to form fullerene-polymer composites, where their special molecular properties are exploited for specific applications. Figure 2.9 illustrates the structure of a fullerene molecule.

Fullerenes, whether forming polymeric solids or fullerene-polymer composites, feature the fullerene molecule as the fundamental building block of the polymeric phase or polymeric composite. The unique structural features of these building blocks result in unique structures and properties. Polymeric fullerenes and fullerene-polymer composites have become interesting for their potential for electronic and optical applications.

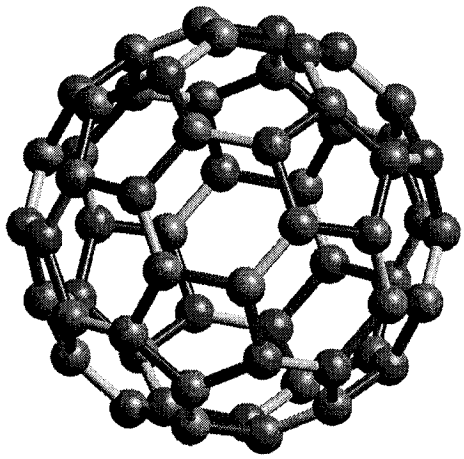

Figure 2.9: Structure of C_{60} molecule

The unusual structure of molecular fullerenes leads to unusual optical, and transport properties. As the structure-properties studies of fullerene-based films proceeded, it was soon demonstrated [41] that, by excitation through photons [41], [42], electron beams [43], plasma discharge [44], pressure [45], and alkali metal doping [46], the films, initially in the crystalline phase, could be transformed into a polymeric phase, with major modifications to their optical, vibrational, and transport properties. Since the early discovery of these effects, extensive studies have been made of the polymeric-induced modifications to the structure and properties of these films [47].

Early demonstration of the potential for the use of small additions of fullerenes to polymers to promote specific optoelectronic applications [48] stimulated much interest and activity, leading to a host of interesting potential applications and to an increased understanding of the transport and optical properties of this fascinating new class of optoelectronic materials.

2.8.1 NANOPARTICLE/CLUSTER FILMS

Recently, films produced by depositing pre-formed mass-selected atomic clusters in the size range 1-10 nm have generated a great deal of interest. The ability to control the size, density and in some cases the morphology of the particles allows unprecedented flexibility in the creation of new types of nanostructures [49]. This section will describe the technology used to produce the particles and deposit them, and discuss the details of the landing on the surface.

The technology to deposit atoms onto well-prepared surfaces in sufficiently good vacuum conditions to enable studies of exposed ultra-thin films has been developed over the previous 40 years and is now at a very high level of sophistication. The ability to freely choose the size of the deposited particles as well as other parameters such as landing energy has enabled the creation of new types of nanostructures with an unprecedented degree of control. In addition, cluster and atomic beams can be combined to produce nanoscale particles embedded in a matrix of different material. Adjusting the deposition rates of the mass-selected clusters and atoms allows independent control of the particle size and volume filling fraction – a feature not available in any other method of granular film production.

Much of the impetus to study supported clusters arises from the enormous technological potential of nanostructured materials, which cuts across several industrial sectors. The novel optical, electronic, magnetic and mechanical properties of the materials whose structure is well defined on the nanoscale ensures that the technology developed to deposit mass-selected clusters will be used in industrial processes within a decade.

2.8.2 CLUSTER SOURCES/PRODUCTION

Cluster sources capable of producing free beams of nanoscale clusters with a wide range of sizes were first reported 20 years ago [50] [51]. The technology continues to develop rapidly, as beam intensities are pushed even higher and new capabilities are introduced such as UHV-compatibility, new mass-selection techniques etc. At the heart of most cluster sources is a region in which supersaturated vapour of the material to be studied and used is generated. With careful design of the nozzle, it is possible to produce clusters containing up to thousands of atoms and phenomenally high deposition rates (~ 1000 Å/s) [52], [53]. In this section, sources that use an inert gas in the cluster production process will be described.

The effect of the presence of an inert gas flow in the condensation region was clearly described by *Sattler et al.* [50] in the first report on this type of source. The Sattler source, which is the prototype gas aggregation source (GAS) is schematically illustrated in figure 2.10.

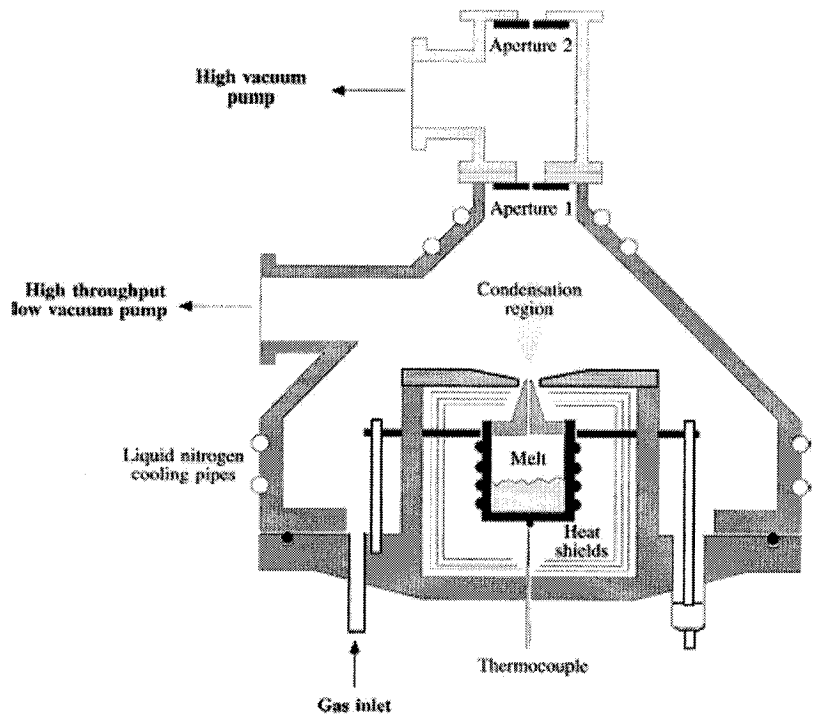

Figure 2.10: Basic layout of the original Sattler source [49]

Its operation will be elaborated on as much of its underlying physics is common to other types of cluster sources available. The heated crucible ejects a vapour through an aperture into a liquid nitrogen cooled, vacuum-pumped region containing He at pressures up to 20 mbar (~ 15 torr). The condensed vapour passes through a pair of apertures into a high vacuum region where it forms a beam of clusters.

2.8.3 CLUSTER FILM MORPHOLOGY AND STRUCTURE

The morphology of thin films made from deposited clusters depends on a number of factors including the substrate and particle materials and temperatures, and the impact energy of the cluster. A detailed description of cluster collisions with surfaces has been given by *Habrich* [54].

Generally, three energy regimes are distinguished for impact energy, i.e. low energy (~ 0.1 eV/atom), medium energy (1-10 eV/atom) and high energy (>10 eV/atom). The difference in the films made by depositing clusters in the different regimes is obvious to the naked eye. Low-energy deposition produces a *sooty*, easily removed film; at the medium energy regime, the film adheres more strongly to the substrate; while high-energy deposition gives a hard, shiny coating. This difference is demonstrated by the molecular dynamics simulations of deposited molybdenum (Mo) clusters on Mo substrates calculated by *Haberland* [55] and shown in figure 2.11.

In the low-energy regime, the clusters suffer little distortion, there is no damage to the surface and the film consists of a highly porous array of randomly stacked particles. The model takes no account of diffusion of the clusters on the surface in between the arrival of new particles, which is reasonable for Mo clusters deposited on a Mo surface [55]. In other systems, however, especially simple metals on graphite, diffusion plays an important and sometimes dominant role in determining the morphology of the film.

At medium energies, the clusters remain intact but their morphology is modified and there maybe some induced defects on the surface. For clusters that are highly mobile on a given substrate, the increased energy may render the particles immobile as a result of the surface damage. At high energies, the clusters are completely disrupted and there is damage to the surface that runs several

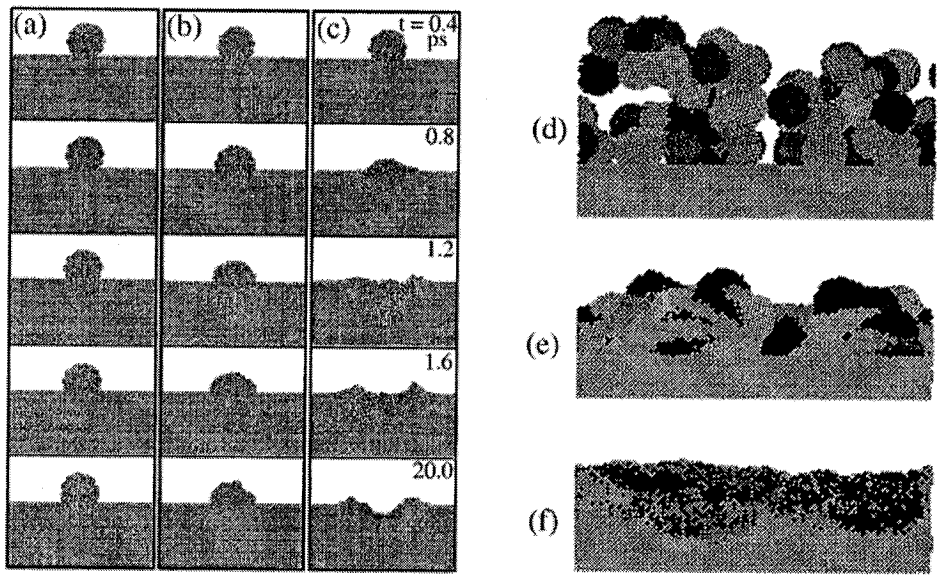

Figure 2.11: Molecular dynamics simulations of the impact of individual Mo clusters and the Morphology of the cluster-assembled films on a Mo(1 0 0) surface as a function of cluster-impact energy: (a,d) 0.1 eV/atom; (b,e) 1 eV/atom; (c,f) 10 eV/atom [49]

layers deep. Although the original cluster is lost in the process, there are technical advantages in depositing high-energy clusters, rather than atoms and ions.

During the free jet expansion phase in the sources based on gas aggregation, the neutral clusters acquire a speed distribution that peaks in the range 50-500 m/s depending on the particle size and type of source. For Fe clusters, for example, this corresponds to 0.1-70 meV/atom, which is well within the low-energy regime. A further reduction can be achieved by thermalizing the clusters with a cold rare gas. Alternatively, they can be ionized and accelerated by applying an electric field for high-energy deposition.

An additional scheme to assist soft landing of clusters is to absorb, at low temperature, a thin rare gas film on the substrate prior to deposition. This acts as an ultra-soft

cushioning layer that is especially useful in the case of very small, mass-selected cluster ions for which it is more difficult to achieve low kinetic energies per atom.

2.9 NANOCOMPOSITE THIN FILMS

The current trend of developing nanophase materials motivates the development of production techniques for nanometer-scale structures in a variety of applications ranging from silicon-based semiconductors, optical coatings and biomedical research to laser and electro-optics. Nanocomposite coatings are the latest interest and are composed of nanocrystalline materials with a grain size of about 100 nm or less. The number of atoms in the grain is comparable to or smaller than that in the boundary region [56]. Thus, properties of nanocomposite films differ greatly from those of microcrystalline films. In recent years, interest in nanocomposite films has grown due to prospective applications of these materials.

Several methods are currently in use for polymer-based nanocomposite production via: (a) the sol-gel technique; (b) in situ intercalative polymerization and; (c) in situ polymerization methodologies. Some plasma-route examples that have been developed are as follows: $GaSb/SiO_2$ nanocomposite films have been synthesized by RF magnetron sputtering for optical devices [57] and TiN/SiN_x films have been deposited by reactive unbalanced magnetron sputtering to improve hardness, wear and oxidation resistance properties of TiN coatings [58]. Whatever the applications investigated, the concept for nanocomposite films is the same: elements that form the film have to be immiscible [59]. Low elaboration temperatures inhibit interdiffusion between the phases that constitute nanocomposite films [60].

2.10 NANOPARTICLE COATING

As reported recently [61], two types of approaches are currently used to produce nanocomposite film containing nanoparticulate fillers: the *in-situ* approach whereby the nanoparticles are synthesized in the polymer matrix from a solution and a second approach which consists of a polymerization of the polymer matrix around the nanoparticles. The first approach generally involves numerous wet-chemical steps and is not well-suited for the deposition of spatially graded films. The second approach involves the use of pre-coated nanoparticles, with the surface layer made up of a material compatible with the host matrix, as precursor materials for nanocomposite fabrication [61].

An innovative concept of using coated nanoparticles as a precursor material for improved nanocomposites is emerging. Compared to materials with grain sizes in the micrometer range, nanomaterials excel in different and new properties. The unique properties of nanomaterials often are properties of isolated particles. After combining nanoparticles to a macroscopic work piece, these unique properties are usually lost. Therefore, in order to obtain macroscopic parts exhibiting properties of the isolated particles, it is necessary to avoid or at least reduce interaction of the particles [62]. This can be achieved by coating individual particles with a second ceramic or polymer layer. By coating nanoparticles with a second layer, the following improvements can be obtained:

- The kernels are kept at a well-defined distance, therefore the interaction of the particles can be adjusted.
- The surface chemistry of the particles can be adjusted according to the needs of application.
- The mixing of the two phases is homogenous on a nanometer scale.

In current research of nanomaterials, it has become critical to modify the surfaces of the nanoparticles both for fundamental research and engineering applications [63-70]. In

previous work, the modification of nanoparticles involved the deposition of ultrathin films (1-5 nm) on the nanoparticles by plasma treatment [71].

The following are images obtained via TEM of nano ZnO particles that have had polymer thin films deposited on them via plasma treatment. As can be seen from the images, the polymeric films form a thin, uniform coating approximately 20 nm in thickness. The polymeric coating can be seen to be well dispersed on the nano ZnO particles giving the particulates defined boundaries and not an agglomerated appearance.

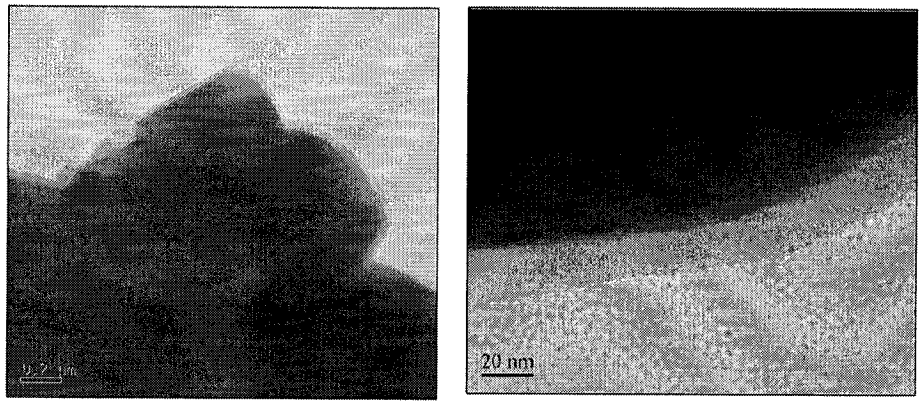

Figure 2.12: TEM images showing acrylic acid coated nano ZnO particles [71]

Nanometric particles are remarkably taxing to handle outside processing reactors due to their inclination to aggregate. A considerable obstacle in nanocomposite thin film production via PECVD is the controlled introduction of the nano-sized filler material into the plasma processing reactor and its eventual incorporation into the polymer matrix.

Particle embedment into thin films can usually be performed via a low-pressure plasma polymerization process accompanied either by a vaporization-condensation process or laser ablation. This brings the desired particles from the sources to the deposition surface [72]. However, the key to homogeneous nanocomposite thin film deposition lies in the contained processing of the nanophase materials. This fundamental aspect will encompass the primary focus of the current thesis study.

3.1 OBJECTIVES

This dissertation's work aims to represent the first steps in the process of development of an innovative approach to the synthesis of fullerene nanoclusters, the coating of such clusters and their incorporation in a plasma polymer thin film. The primary objective of this project is to devise and implement a PECVD system for the co-deposition and study of a polymer matrix and nanometric sized filler particles, in effect, yielding nanocomposite thin films. Furthermore, the possibility of coating nanoparticles with a thin film prior to deposition in the polymer matrix would be studied along with the effect of nanoparticle surface functionalization. The various elements of this research project can be divided into three phases which are categorized as follows:

1- Design
   (a) Design and implement a reactor configuration with a substrate holder (allowing freedom of axial movement) and auxiliary equipment necessary for plasma processing
   (b) Design and implement a particle injector scheme for the synthesis and introduction of the nanoparticles to the reaction chamber
2- Experimental
   (a) Deposition of plasma polymerized films
   (b) Deposition of filler material (C_{60}) films
   (c) Co-deposition of plasma polymerized films and filler material
3- Characterization
   (a) nanoparticles
      - Structure (TEM)

   (b) films
      - Structure: *(i)* Thickness (surface profilometer)
        (ii) Surface Topography (OM, SEM, TEM)
      - Composition: FTIR-ATR

4.1 EXPERIMENTAL APPARATUS

Many experimental arrangements have been cited in the literature, each differing mainly in: the type of power supply used and; reactor geometries [35]. Figure 4.1 depicts a schematic overview of the experimental setup utilized in the current research. This can be split into three regions as follows: *(i)* precursor gas dispensing system – comprising of argon (Ar) and ethane (C_2H_6) gas cylinders in line with rotameters to regulate the flow rate of gases to the reactor; *(ii)* reactor setup – comprising of a particle (C_{60}) injector, a quartz, tubular reactor and a substrate holder connected to a RF Power supply to produce the necessary electromagnetic field; and *(iii)* exhaust system – comprising of a rotary pump.

The rationale that led to the development of this process consists of four aspects: i) Fullerenes, C_{60}, have a significant vapor pressure at modest temperatures [73]. ii) Fullerenes, C_{60}, are inclined towards polymerization through the formation of covalent bonds between cages but also tend to react readily with organic groups [74 Thus, C_{60} nanoclusters of desired size can potentially be synthesized by carefully controlling the residence time of the fullerenes, C_{60}, in a nanocluster formation zone prior to their exposure to a surface coating process. iii) When injected into a weakly-ionized plasma and exposed to the electron gas, fullerene C_{60} molecules will develop a negative floating potential due to the build-up of surface charges [75 The repulsive electrostatic force that develops amongst C_{60} particles (or nanoclusters) is expected to play a role in the formation of small-sized nanoclusters in the plasma environment by inhibiting (or slowing down) the agglomeration process caused by weak van der Waal interaction forces. iv) Plasma polymerization reactions involving a foreign monomer gas reacting with the C_{60} nanoclusters will terminate their growth by encapsulation, and give rise to an isolation of the nanoclusters from each other. The conditions leading to plasma polymerization onto nanoparticles is readily achieved using a monomer gas which produces the methyl radical upon dissociation in the plasma environment [76

The monomer gas utilized is ethane as it has been widely studied in the domain of plasma polymerization [77], [78] and is supplied by Scott Speciality Gases with a purity of 99%. The inert carrier gas opted for is argon, ultra high purity, and is supplied by MEGS Inc. The filler material utilized is buckminsterfullerene (C_{60}) due to reasons stated previously in the literature review section and it is obtained in a mixed fullerene format from MER Corporation with a composition as follows: 75% C_{60}, 22% C_{70} and 3% higher fullerenes. The substrate materials utilized were silicon and quartz discs, 1 inch in diameter. The silicon discs were purchased from Silicon Valley Microelectronics, Inc. and were virgin test grade with a: P/Boron dopant; <100> orientation; 1-20 Ω-cm resistivity; 250-350 μm thickness; and with one side polished. The quartz discs were purchased from Technical Glass Products, Inc. and were made of Corning type 7980© fused silica.

A micro-Pirani pressure transducer, type 910 from MKS, was utilized to monitor the pressure within the system. The power generator utilized was model RFX600A from Advanced Energy Inc with an output power capacity ranging from 6 to 600 watts. An AZX 10 high frequency matching network was used together with a TCMII controller from Advanced Energy Inc. in order to provide load matching between the power supply unit and the plasma system. A DASO8-Jr data acquisition board was utilized with LabVIEW graphical and development software from National Instruments in order to create a graphical user interface for the acquisition of particle injector temperature and reactor pressure data from the setup.

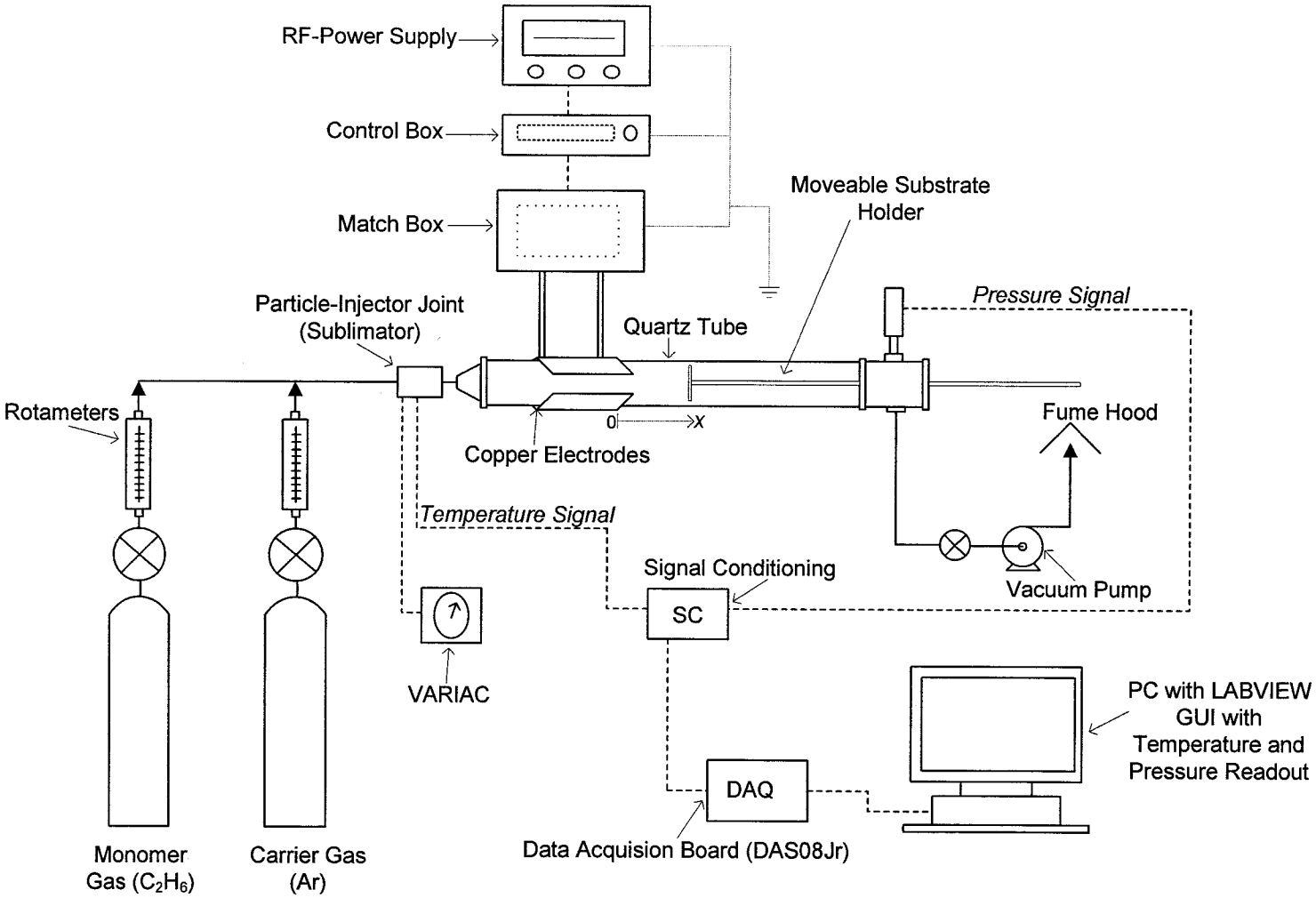

Figure 4.1: Schematic Overview of Experimental Set-Up

4.2 REACTOR DESIGN

Figure 4.2 illustrates the schematic of the RF-discharge reactor utilized. The body of the reactor was made using a quartz tube with an internal diameter of 1.5" (3.81cm), external diameter of 1.66" (4.21 cm) and a length of 24" (60.96 cm). The reactor setup was arranged in a horizontal fashion with a stainless steel head flange and an acrylic downstream flange which supported the pressure transducer, the substrate holder and the hose leading to the vacuum system.

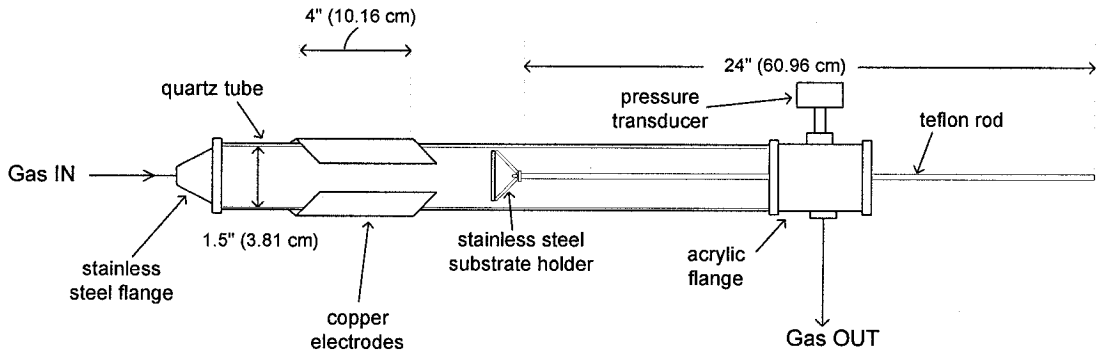

Figure 4.2: Detailed illustration of RF-discharge reactor utilized

The support rod for the holder is fabricated from Teflon®, as it is an electrical insulator and has a higher melting point than acrylic (melting point of Teflon = 220 °C / 493 K; melting point of acrylic = 130 °C / 403 K) and the holder itself is made from stainless steel. The substrate holder is moveable, hence allowing for axial substrate position freedom and is centered with the axis of the reactor. The plasma gas and nanocluster stream impinges on the substrate positioned normal to the flow. The electrodes consist of two brass metal sheets wrapped around the quartz tube and located 1 cm downstream of the stainless steel flange. The upper electrode is connected to the rf power unit while the lower one is connected to the rf power unit's ground. A brass box (not shown in the figures above) which acts as an EMI (ElectroMagnetic Interference) shield is placed on the reactor.

4.3 PARTICLE INJECTOR DESIGN

The basic function of such a device is to: (i) sublime raw material (fullerene, C_{60}, in the present study); (ii) allow for residence time modulation in nanocluster formation zone and; (iii) transport clusters into the reactor. The motivation for the particle injector design is from the gas aggregation source quoted by Heer at al. [79] and is illustrated in figure 4.3.

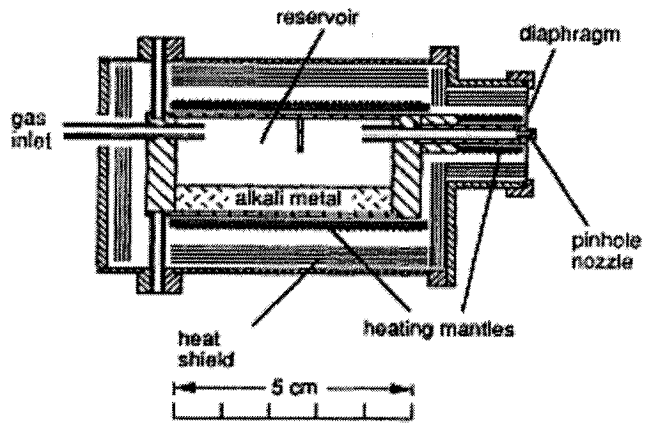

Figure 4.3: Seeded gas aggregation source [49]

The principle of operation of the seeded gas aggregation source follows that the crucible containing the cluster source is heated until the sample sublimates. This vapour is then mixed with (seeded into) a carrier gas introduced at a pressure of several atmospheres and is then transported away into the reaction chamber. The design adapted and implemented for the particle injector is illustrated in figure 4.4 and it follows the same ideology.

The cylindrical shell enclosing the heaters is made of brass and surrounded by a ceramic insulating wool. The heaters (four) are CIR-2025/120 V cartridge heaters purchased from OMEGA. A tubular quartz piece, 11 mm in internal diameter and 50 mm in length inserted within furnace, was made with a side gas inlet and in order to accommodate the sample. This piece was attached to a stainless steel flange purchased from Kurt J. Lesker

Inc. using a cajun nut. The flange was attached to a similar one at the inlet of the reactor

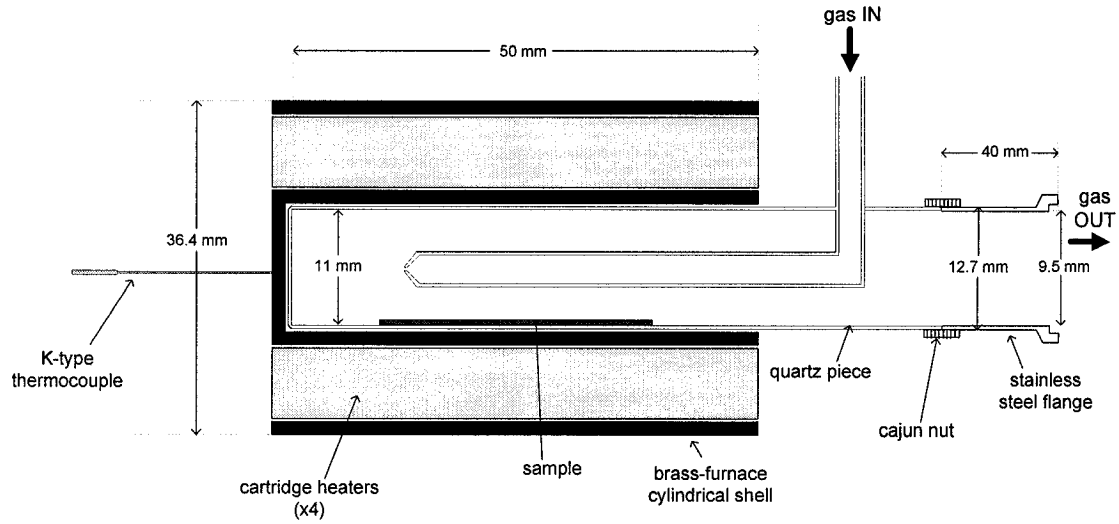

Figure 4.4: Lateral view of particle injector

using an o-ring and clamp configuration. Figure 4.5 gives a cross-sectional illustration of the injector showing the concentric arrangement of pieces.

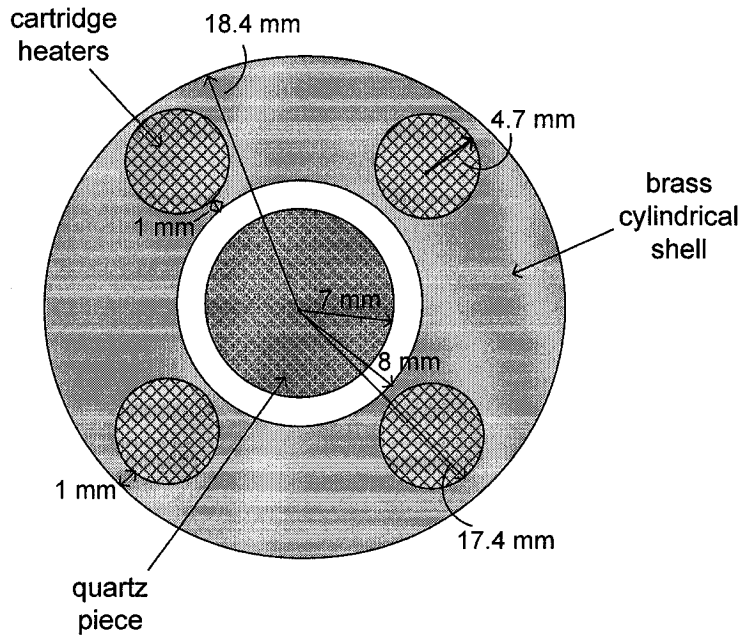

Figure 4.5: Cross-sectional view of particle injector

4.4 PROCESS PARAMETERS

Experimental conditions utilized were narrowed down using the results of Hiratsuka et al. [80] who used a similar parallel-plate-electrode, tubular reactor configuration as the one utilized in this project. Several studies were conducted by him studying the effect of monomer flow rate (sccm/min), input power (W) and pressure (torr) on molar deposition rates (mole/min.cm^2) for several different monomer gases such as methane (CH_4), ethane (C_2H_6) and propane (C_3H_8). The main results obtained and of relevance to the project are illustrated in the following plots.

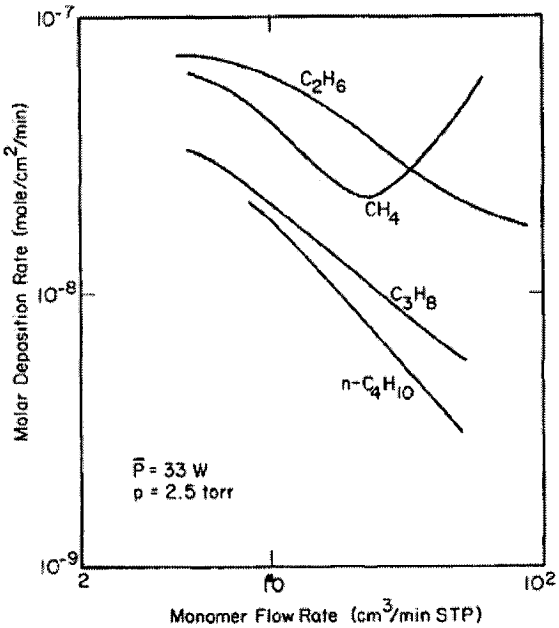

Figure 4.6: Molar deposition rate for plasma polymerization of methane, ethane, propane and n-butane at 33 W and a pressure of 2.5 Torr plotted as a function of monomer flow rate [80]

Figure 4.6 shows the molar rates of polymer deposition as a function of the rate of monomer supply at fixed power level and pressure. The deposition rates follow a similar trend and are in the following order: C_2H_6>C_3H_8>C_4H_{10}. For ethane, propane and *n*-butane, the deposition rates decrease with increasing flow rate with methane being anomalous in behaviour. It exhibits an initial decrease in deposition rate to a minimum and then increases with flow rate. The general trend of decreasing deposition rates with increasing monomer feed rate is consistent with that observed in the plasma

polymerization of other monomers [81]. The interpretation is that the residence times of the reactive species is decreased by an increased flow rate and that some of the reactive species are swept away before polymerization can take place. The next illustration, figure 4.7, shows the deposition rate data for the same four monomers as a function of power input. Due to an increase in power input, a larger number of active species are present in the plasma and this leads to an enhancement of the rates of deposition.

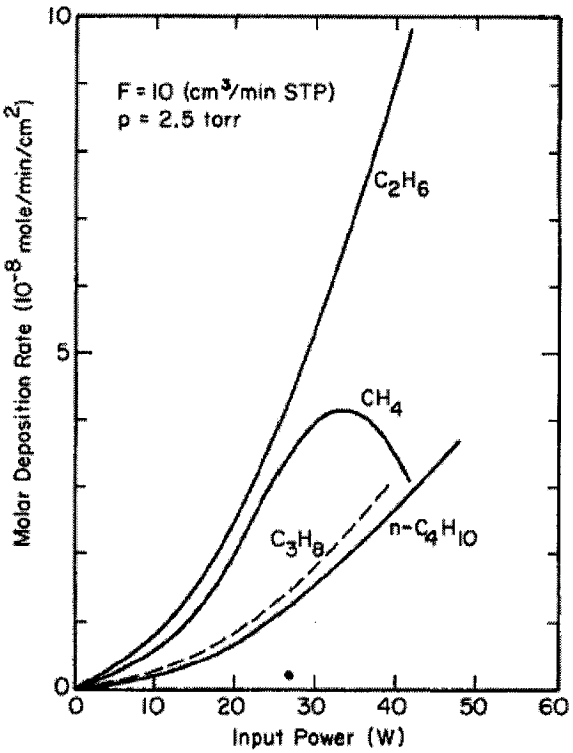

Figure 4.7: Molar deposition rate for plasma polymerization of methane, ethane, propane and n-butane at a flow rate of 10 sccm/min and a pressure of 2.5 torrs plotted as a function of input power [80]

Using the criterion of higher molar deposition rates, the monomer gas of choice is ethane. Hiratsuka further went on to obtain the *characteristic map* for the plasma polymerization of ethane (see figure 4.9). It was found that the form of the plasma polymer may be oil, film or powder [82]. Two competing processes are operative: one is the rate of propagation in the gas phase, and the other is the rate of diffusion of the active species to the electrode region from the plasma. If the polymerization rate is high, then the homogeneous reactions dominate in the gas phase to form powdery products. On the other hand, if the diffusion rate is greater, then the heterogeneous reactions on the substrate surfaces yield films and/or oils.

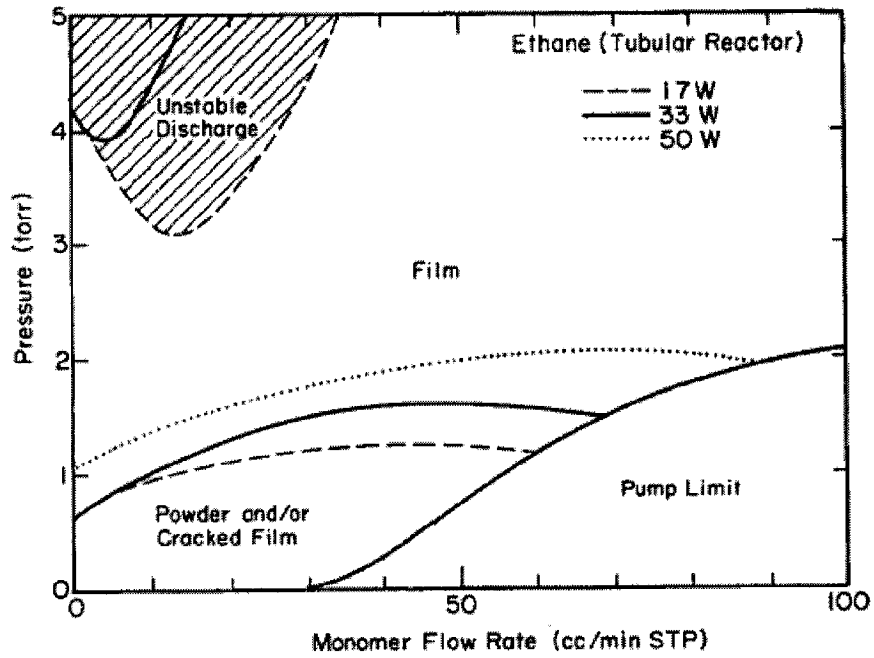

Figure 4.8: Characteristic map for plasma polymerization of ethane in a tubular reactor [80]

For ethane, all three forms of plasma polymer can be obtained [81]. As ethane polymerizes slowly in the plasma, films are formed under most conditions. Only at very low pressures and flow rates can partial formation of powder be observed. The regions of powder formation are enlarged with increasing power input because of the enhanced population of active species. On the other hand, the regions of unstable discharge shrinks with increasing power, being negligible at 50 W. At high rates of polymerization, the powdery products in the gas phase act as electron sinks, thus rendering it difficult to sustain the discharge.

After experimenting with different values of monomer flow rate, reactor pressure and input power and using figure 4.9 as guidance, the following values were selected as the operating parameters utilized in experimentation for the results presented next:

- *Monomer flow rate*: 25 sccm
- *Pressure*: 1-2 torr
- *Plasma power*: 30 watts
- *Argon flow rate*: 25 sccm
- *Substrate position*: 1 cm (after tail-end of electrode)

- *Sublimation temperature*: 500 - 650 °C
- *Polymer deposition time*: 10 – 20 minutes
- *Fullerene film deposition time*: 15 minutes

4.5 EXPERIMENTAL PROCEDURES

I- Plasma Polymerization

The start-up procedure was routine and accomplished in the following manner. The substrate would be cleaned with acetone and mounted on the substrate holder. The downstream flange with the substrate holder would then be affixed to the reactor. The pressure transducer and hose leading to the pump would then be connected to this downstream flange. Finally, the upstream flange would be connected to the gas supply, the substrate position finalized and the system would then be ready to be pumped. After allowing it to evacuate for 30 minutes, the base pressure obtained would be 8 mTorr under typical conditions.

The substrate would then be exposed to an argon plasma at an argon flow rate of 100 sccm and power input of 30 watts for a duration of 5 minutes in order to further remove *in-situ* any contaminants left on it prior to polymer deposition. After which, the flow rate of the monomer would be established at 25 sccm and the pressure regulating valve, connected just before the pump, would be adjusted until a final operating pressure of ~ 1 torr would be obtained. The glow discharge would then be ignited at an input power of 30 watts and the experiment carried out for the duration of the deposition time.

At the end of the experiment, the rf power would be turned off and the monomer gas flow rate would be allowed to run for 5-10 more minutes in order to eliminate radicals possibly present on the plasma-polymer film surface. The gas flow would be then turned off and the system allowed to come to atmospheric pressure by closing the vacuum valve and slowly dismantling the pressure transducer joint. The substrate disc would then be stored away in a labeled Petri dish, pending further diagnostical analysis. Experiments were carried out on both quartz and silicon substrates and a film thickness study was carried out for deposition times of 10, 15 and 20 minutes in order to study the plasma-polymer film growth using the current reactor configuration.

II- Fullerene (C_{60}) Film Deposition

The start-up procedure for mounting the substrate is as described before. The substrate would be positioned at the furthest end of the reactor and before evacuating the system, the particle injector would be loaded with 500 mg of the fullerene mixture and attached to the upstream flange of the reactor. The system would then be evacuated for 30 minutes until it reached the base pressure of around 8 mTorr. The carrier gas flow rate (argon) would then be established at 25 sccm and a glow discharge would be ignited at 30 watts and a pressure of ~ 1 torr. The heating cartridges present in the particle injector were connected to a VARIAC used to alter the heating rate which, in turn, is used to adjust the temperature of the fullerene extract. The temperature of the heater would be ramped up to -50 °C (*standby temperature*) of the final/desired temperature (i.e. if it was desired to be at 550 °C, the furnace would be brought to a temperature of 500 °C) while the substrate would be placed at the far end of the reactor away from the particle/gas inlet.

It would then be allowed to remain at that temperature for 10 minutes in order to establish a temperature uniformity within it. The temperature would then be ramped up to +50 °C of the final desired temperature during the deposition time allotted for the experiment (i.e. if it was desired to be at 550 °C and the deposition time was 10 minutes, the furnace would be brought to a final temperature of 600 °C within 10 minutes. From this, it was roughly assumed that the average temperature of the furnace, during deposition time, would be 550 °C). Simultaneously, the substrate would be brought forward to its desired position while the temperature is being ramped up.

After deposition would be over, the heaters would be turned off and the substrate rapidly retracted to the furthest end of the reactor in order to ensure that minimal deposition of fullerenes occurs on it outside of the deposition time. Consequently, blank runs would be conducted, with the substrate always positioned at the furthest end of the reactor, to check if there was deposition happening at that position. It was confirmed under an SEM that deposition was almost negligible at that distance. At the end of the run, the gas flows

would be turned off and the furnace cooled down. The system would then be brought to atmospheric pressure and the substrate disc would be stored away in a labeled Petri dish, pending further analysis.

III- Co-Deposition of Polymer and C_{60} Clusters Film

The procedure followed is an amalgam of the abovementioned ones and the actual deposition is done in three steps as illustrated in figure 4.10. The start-up procedure for mounting the substrate and loading the fullerene mixture is as before. The system would be brought to base pressure as previously described and the substrate would be cleaned in situ using an argon plasma.

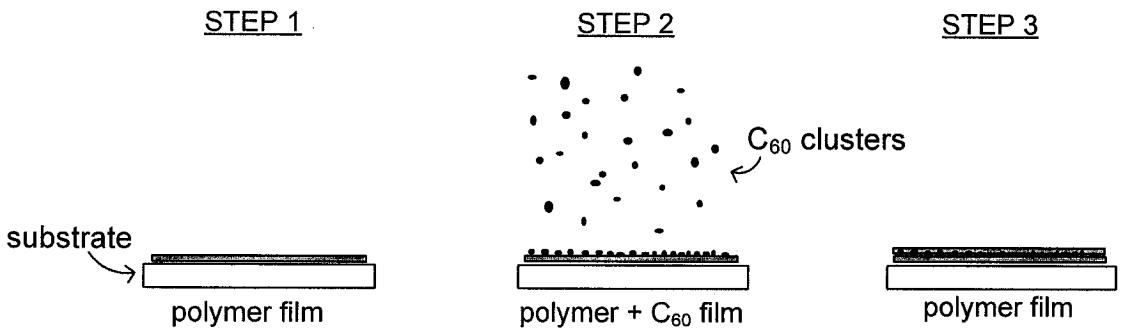

Figure 4.9: Deposition steps of the polymer-fullerene composite films

Before deposition of the polymer film, the temperature of the furnace would be brought to -50 °C of the desired temperature as before. In step 1, a polymer film would be deposited for 10 minutes, followed by step2, in which a polymer and fullerene film would be simultaneously deposited, and finally, in step 3, another polymer film would be deposited for 10 minutes giving way to a sandwich-type mechanism for the deposition of the composite film. At the end, the furnace would be allowed to cool down and the system brought back to atmospheric pressure. The substrate would be stored in a labeled Petri dish, awaiting further analysis. Fullerene samples were also collected from the reactor walls for analysis in order to examine the effects of exposing the sublimate to an inert and reactive (ethane) plasma and also to study the morphology of the samples.

4.6 POST-DEPOSITION ANALYSIS

The structure of the films was examined at different levels of spatial resolution. A shadow mask was utilized during the deposition of the plasma polymerized films in order to define an edge to the film on the substrate. The thickness was then determined directly using the Dektak^{3}ST surface profilometer. The principle of operation of the profilometer is the dragging of a stylus across a film while measuring stylus vertical deflections to a maximum extent of about 1nm. The films were visually analyzed using a Nikon EPIPHOT 200 optical microscope bundled with a JS 2000 CLEMEX-vision image analysis software to capture images. Images were obtained at magnifications ranging from x50 up to x1000.

The microstructure and morphology of the films obtained was discerned by micrographs of the films under a scanning electron microscope (FEGSEM, Hitachi 3000). Furthermore, the structure of the solid particulate deposits exposed to the reactive ethane plasma and collected from the reactor walls was analyzed using a transmission electron microscope, TEM (JOEL JEM-2011 with a FasTEM and a Gatan 300W 1.3 K x 1.0 K CCD camera).

The composition of the films was determined using FTIR-ATR analytical techniques. ATR, acronym for attenuated total reflectance, is also known as internal reflectance spectroscopy (IRS) or multiple internal reflectance (MIR). It is a versatile, nondestructive technique for obtaining the infrared spectrum of a material that is either too thick or too strongly absorbing to be analyzed using standard transmission spectroscopy. It is a widely used technique for the analysis of polymer samples with low transmission [83]. In the present situation, the substrate materials utilized (quartz and silicon) were heavily absorbing in nature in the wavenumber region of interest.

5 RESULTS

The following sections elaborate on the results obtained from the characterization tests conducted on the nanoparticles and films produced. The results are presented initiating off at the macroscopic scale and exploring towards higher magnification with SEM and TEM results. The first set of results presented is from the thickness measurement studies of the plasma polymerized polyethylene films. This test was carried out primarily to obtain a polymer film deposition time to be used in consequent experiments and to probe into the mechanism of plasma polymer film growth. That is followed by a compositional study of the polymer and fullerene films obtained using FTIR-ATR analysis. This is carried out in order to determine the formation of polymer films obtained from the procedure utilized. More importantly, the results are used to determine whether molecular fragmentation of the C_{60} occurs via the sublimation route opted for. The mesoscopic surface topography of the fullerene films was analyzed utilizing an optical microscope. The images obtained are presented followed by a characterization of the percentage coverage of the substrate surface by the fullerene films. An attempt is made to fit a model to the data obtained and this is presented in the ensuing section. In order to study the morphology of the particles acquired via the action of the reactive ethane plasma on the in-flight sublimated C_{60} particles, TEM analysis is carried out on samples collected from the reactor tube deposited around the electrode region. The results obtained are compared with TEM micrographs of untreated C_{60} samples. Lastly, the surface morphology of the nanocomposite coatings fabricated is analyzed using an SEM. The results obtained from the electron microscopy study are used to study the effect of the monomer gas on the particles and deduce a probable coating formation mechanism.

5.1 THICKNESS TESTING

Polymer films were prepared at an input power of 30 watts, operating pressure of 1 torr and monomer flow rate of 25 sccm. Deposition times, $t_{deposition}$, of 10, 15 and 20 minutes were experimented with. The thickness of the polymer films was measured using a

Dektak^{3}ST surface profile measuring system and the resulting observations can be seen in figure 5.1.

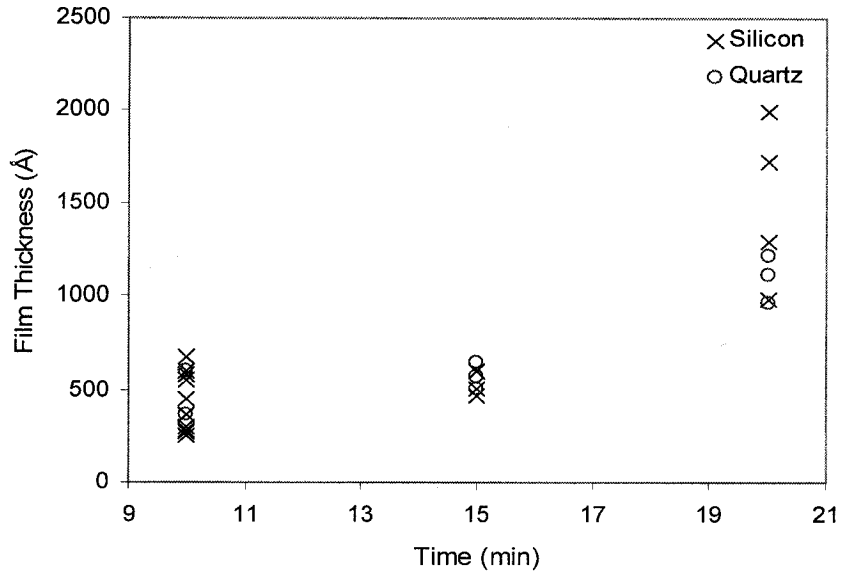

Fig 5.1: Film thickness of plasma polymerized polyethylene, in Å, versus deposition time, in minutes

Each data point represents the averaged value of 15 thickness measurements per disc taken randomly across the entire length of the polymer film. The standard deviation of values of film thickness at a deposition time of 10 minutes is σ_{t10} = 162 Å while this number is 70 Å and 290 Å at deposition times of 15 and 20 minutes respectively. A greater spread is observed at the lower and upper time values of 10 and 20 minutes. The results of the experimental conditions tested give an insight into a possible growth mechanism of the polymer film and this can be schematically portrayed in figure 5.2.

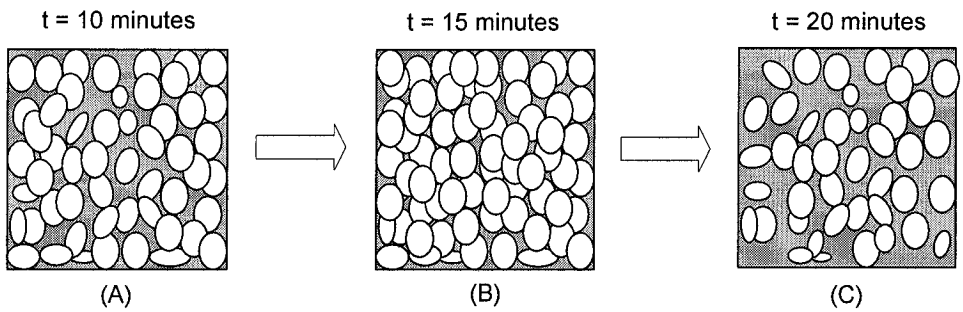

Fig 5.2: (a) island like growths; (b) percolation of islands; (c) burning off of film

The proposed mechanism starts off with island like growths that percolate to form a relatively smooth film followed by burning off of the film at higher deposition times due

to local heating of the substrate surface as it becomes more thermally insulating. The presence of the island-like film deposits is apparent in SEM images obtained of the polymer films and presented later in this chapter under SEM analysis. However, in order to validate this proposed mechanism, further tests need to be carried out at a multitude of deposition times.

5.2 COMPOSITION ANALYSIS

The technique utilized to characterize the composition of the polymer and fullerene deposits obtained was Fourier transform infrared spectroscopy (FTIR) implemented via transmission sampling. This was coupled with the surface sensitive technique of attenuated total reflection (ATR) due to the opaque nature of the substrates. FTIR-ATR is a versatile technique used to measure a physical property of matter and relating the data to the corresponding chemical composition. The physical property measured is the ability of matter to absorb (absorbtivity), transmit (transmitivity) or reflect (reflectivity) infrared radiation. Figure 5.3 shows the results from the IR absorption spectra obtained using FTIR-ATR.

Fig. 5.3(A) is the spectrum of a pure polyethylene film manufactured by 3M Corp. and 100 μm in thickness. Fig. 5.3(B) is the spectrum of the polymer film deposited on a substrate under typical experimental conditions. Peaks of interest that coincide are the C-H rock and bend matches at the wavenumber region around 3,000 and 1,470 cm^{-1}. Lack of C-H stretch bands beyond the 3,000 cm^{-1} wavenumber indicates lack of unsaturation. The spread of peaks indicates amorphousness and polydispersity in the film structure which is to be anticipated considering the mechanism of film build-up. Several film growth mechanisms take place in the plasma of saturated hydrocarbons which consequently leads to the amorphous nature of the resulting films [84].

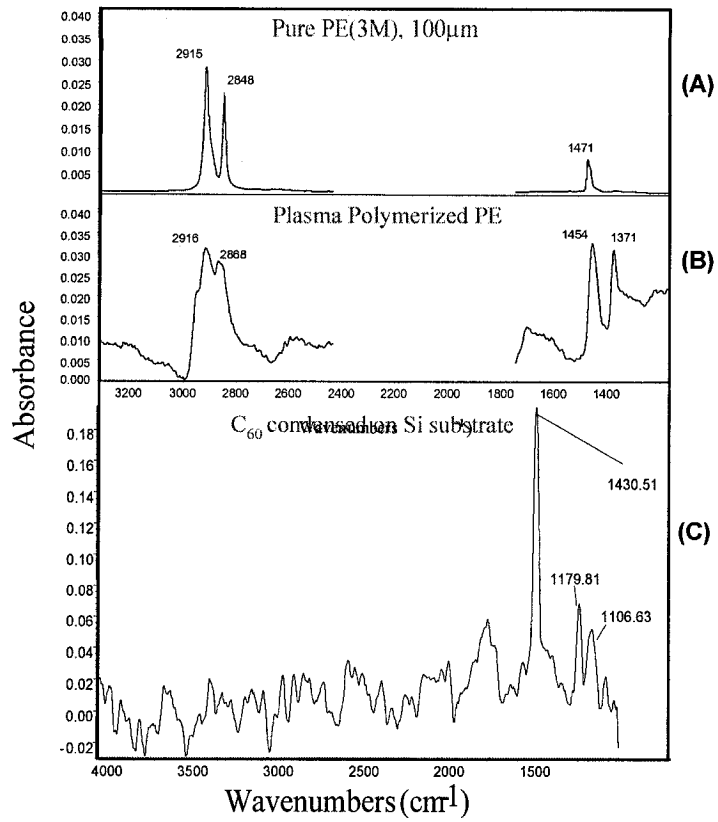

Fig 5.3: Absorbance spectra of: (A) pure polyethylene film; (B) plasma polymerized polyethylene film; (C) fullerene cluster film

Fig. 5.3(C) is the spectrum obtained from the fullerene film deposited via sublimation and condensation in an inert argon plasma. It features the typical peaks of molecular C_{60} at wavenumbers of 1,430, 1,179 and 1,106 cm^{-1} [85]. This confirms that at least some of the fullerene molecules are not fragmented via the sublimation process and on exposure to a weakly ionized plasma.

It is also worth mentioning that, while monitoring the visible optical emission from the argon plasma seeded with the fullerenes using a low-resolution spectrometer (Ocean-Optics USB2000) equipped with an optical fiber, there was no significant optical emission from the C_2 Swan band around 516 nm observed. The C_2 molecule, being a building block for the formation of fullerenes, is expected to be present in the plasma phase if fragmentation occurred. This further affirms the abovementioned inferences.

5.3.1 PROCESSING OF OPTICAL MICROSCOPE (OM) RESULTS

The polymer and fullerene films obtained were further analyzed using a Nikon EPIPHOT 200 optical microscope bundled with a JS 2000 CLEMEX-vision image analysis software to capture images. Images were taken at magnifications ranging from x50 down to x1000 for both quartz and silicon substrates. The following is an example of images captured on substrate discs masked during deposition in order to obtain a contrasting sample with uncoated and coated regions, for purposes of film thickness measurements.

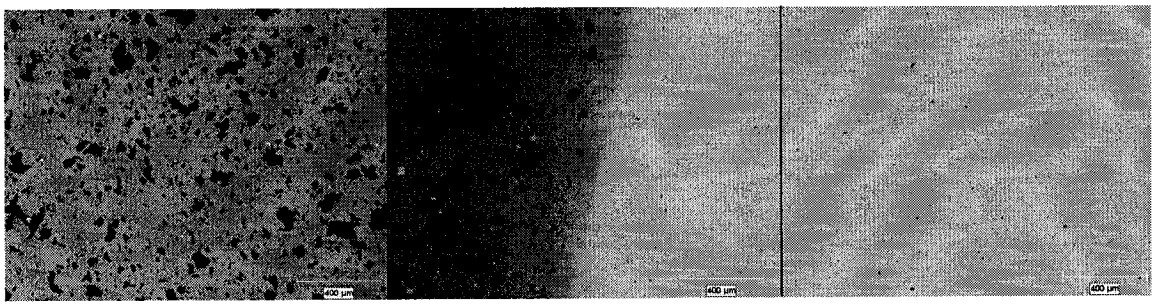

Fig 5.4: Contrasting image obtained with a polymer + fullerene coating on the extreme left, followed by the partition of the two regions and consequently, the uncoated region on the right. Magnification – x50; Scale – 400μm.

These images show a uniform dispersion of the fullerene particles on the substrate surfaces. Furthermore, agglomeration of the particles into clusters is visible. An interesting outcome of the optical analysis was the characterization of the percentage-coverage of discs with the fullerene films at varying temperatures. The procedure of the characterization process developed is explained in the following section.

5.3.2 OBTAINING PERCENTAGE COVERAGE

For the fullerene-island-film (FIF) discs, multiple images were captured at random sections of the discs using a constant magnification of x500 (yielding a scale of 400 μm). The following is an example of images captured from the disc obtained at a sublimation temperature of 600 °C and deposition time of 10 minutes.

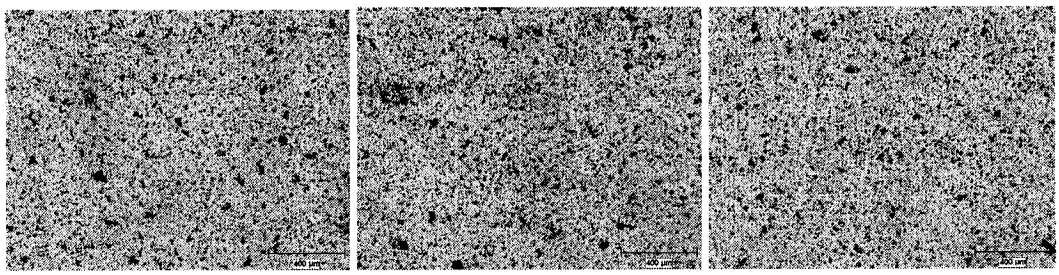

Fig 5.5: Random images captured of the fullerene-island-films at T = 600 °C; magnification = x50

The images obtained from all the FIF discs show a similar black and white pattern with the only observable variable being the ratio of the black spots (being C_{60}) to the empty white spaces with respect to the sublimation temperatures, T_{sub}. As a contrasting example, the following are sample images captured from discs obtained at sublimation temperatures of 500 °C and 650 °C.

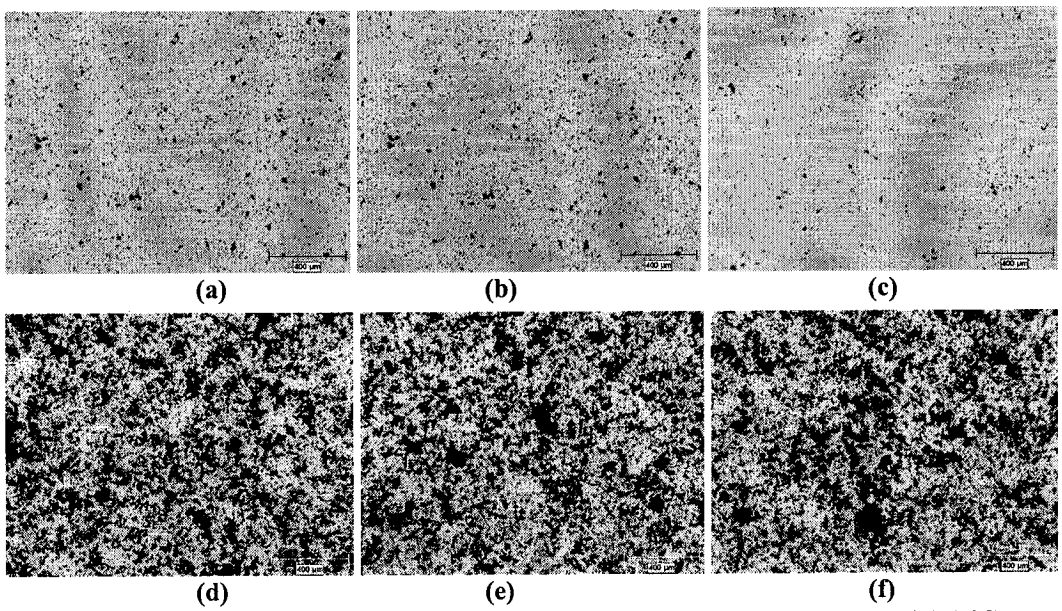

Fig 5.6: a-c = images obtained at a T_{sub} of 500 °C. d-f = images obtained at a T_{sub} of 650 °C

The images obtained were then analyzed using the SCION Image processing and analysis software. The software was used to analyze the percentage black pixels in the image as opposed to white. This was then approximated to be equal to the percentage-fullerene-coverage of the substrate discs. The images were first converted to binary format and then a macro was programmed and launched to calculate the percentage area taken up by the black pixels. The following figure is an example of such an operation.

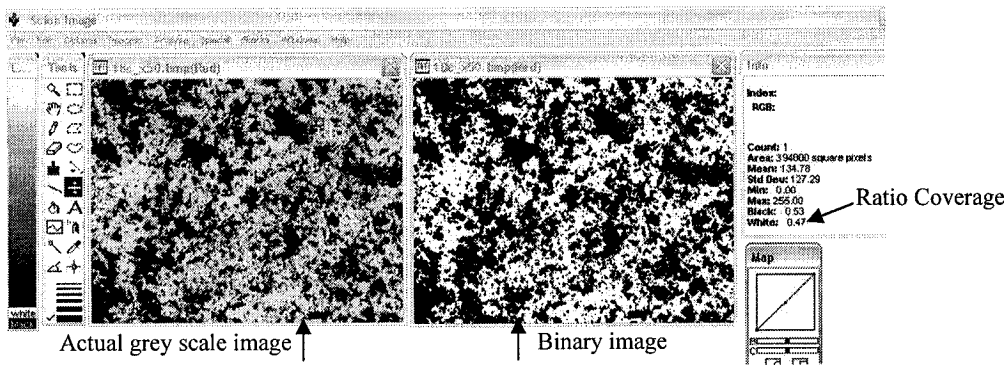

Fig 5.7: Example software usage screenshot for calculation of percentage coverage by C_{60}

The resulting plot obtained for percentage fullerene coverage with respect to sublimation temperatures (ranging from 500 – 750 °C) is shown in figure 5.8. Data points below 500 °C were approximated to have negligible percentage coverage whereas those above 800 °C were approximated to have complete coverage based on data from fullerene vapor-pressure curves [86]. We obtain a sigmoidal relation which can be anticipated as percentage coverage is a function of the flux of particles arriving to the substrate surface which, in turn, is a function of the vapor pressure of the C_{60} particles. In the lower temperature zone (T_{heater} < 500 °C), we anticipate to see minimal coverage due to the low vapor pressure (< 10^{-6} Torr) exhibited by the C_{60} molecules in that zone. At moderate temperature zones (500 °C < T_{heater} <750°C), the vapor pressure increases up to 0.5 mTorr. At heater temperatures within this region, we see a rapid increase in percentage coverage, for the fixed deposition time of 10 minutes, as the C_{60} vapor pressure crosses the minimal vapor pressure threshold, set by the system pressure, for substantial sublimation to occur. At higher temperatures, there is a higher flux of sublimated particles arriving at the substrate surface and hence the percentage coverage is seen to increase rapidly. At temperatures upwards of 850 °C, the vapor pressure is above 20 mTorr and therefore, we can assume a near-complete coverage of the substrate surface which is consistent with the higher vapour pressure.

The sigmoidal relation observed is typical in: material failure analysis studies of applied stress on strain [87]; population growth analysis [88] and; traditional reliability analysis [89]. Such analysis are based on techniques centered on *time*-to-*failure* data and can analogously be applied to the present case of *sublimation temperature*-to-*percentage*

coverage data. The Weibull distribution is abundantly used in model-fitting of failure analysis study data and, consequently, an attempt was made to fit it to the current data to validate the abovementioned assumption and to pave the way for future model-predictors of percentage coverage as a function of sublimation temperature. The model can be given an added depth of dimensionality by factoring in the variable of deposition time as well, which was kept fixed at 10 minutes for the purpose of this study. The following sections give a concise background on the theory of the Weibull distribution and some of the common methods utilized for parameter estimation.

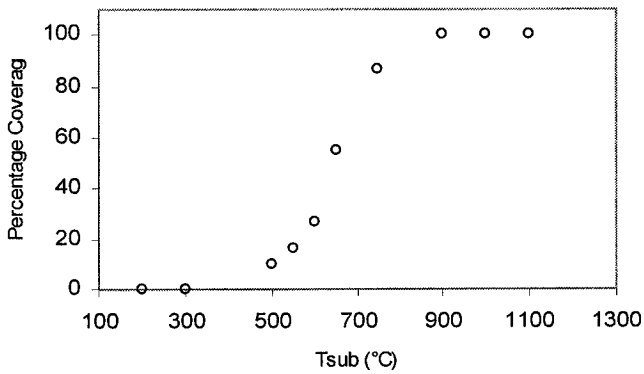

Fig 5.8: Percentage coverage versus T_{sub} at a deposition time of 10 minutes

5.3.3 THEORY OF THE WEIBULL DISTRIBUTION

Selecting a model of the right form to fit a set of data usually requires the use of empirical evidence in the data, knowledge of the process and some trial and error experimentation. For the purpose of the current data set, the Weibull distribution was found to be a good-fit. The Weibull distribution is one of the most widely utilized lifetime distributions in reliability engineering. It is a versatile distribution that can take on the characteristics of other types of distributions, based on the value of the shape parameter, β. The Weibull distribution has a relatively simple distributional form, however, the shape parameter allows it to assume a wide variety of shapes. This combination of simplicity and flexibility in the shape of the Weibull distribution has made it an effective distributional model. The three-parameter Weibull probability density function (*pdf*) is given by the following expression:

$$f(T)=\frac{\beta}{\eta}\left(\frac{T-\gamma}{\eta}\right)^{\beta-1} e^{-\left(\frac{T-\gamma}{\eta}\right)^{\beta}} \quad (1)$$

$$f(T)\geq 0,\ T\geq 0 \text{ or } \gamma,\beta>0,\eta>0,-\infty<\gamma<\infty$$

Where:

η = scale parameter

β = shape parameter (or slope)

γ = location parameter

The two-parameter Weibull *pdf* is obtained by setting $\gamma = 0$ and is given by:

$$f(T)=\frac{\beta}{\eta}\left(\frac{T}{\eta}\right)^{\beta-1} e^{-\left(\frac{T}{\eta}\right)^{\beta}} \quad (2)$$

The one-parameter Weibull *pdf* is obtained by setting $\gamma = 0$, and assuming β = C = constant = assumed value. The expression is then given by:

$$f(T)=\frac{C}{\eta}\left(\frac{T}{\eta}\right)^{C-1} e^{-\left(\frac{T}{\eta}\right)^{C}} \quad (3)$$

Here, the only unknown parameter is η. Note that in the formulation of the one-parameter Weibull, it is assumed that β is known a priori, from past experience on similar or identical products. The advantage of doing this is that data sets with few or no failures can be analyzed.

Due to its flexible shape and ability to model a wide range of data kinds, the Weibull has been used successfully in many applications as a purely empirical model. The Weibull distribution can be derived theoretically as a form of Extreme Value Distribution[2],

[2] These are the limiting distributions of the minimum or maximum of a very large collection of random observations from the same arbitrary distribution.

governing the time to occurrence of the 'weakest link' of many competing failure processes. This explains why it has been successful in applications such as capacitor, relay and material strength failures which can be made analogous to the present study of percentage coverage. The purpose of fitting this model to the data is to obtain a relationship between the percentage coverage and sublimation temperature.

5.3.4 MODEL-FITTING TO EXPERIMENTAL DATA

In the present work, the Weibull distribution is employed to analyze the experimental data on percentage-fullerene-coverage. The method utilized for parameter estimation is via graphical means using the Weibull Probability Plotting procedure (refer to the appendix for a concise description of miscellaneous methods for parameter estimation). The location parameter, γ, which simply translates the distribution spread relative to the standard normal distribution, is assumed to be zero in order to truncate the three parameter cumulative Weibull distribution function to two parameters which is a common practice for the sake of simplicity without losing attention to detail [90]. The *observations* are measured in temperature units (T, °C) and the resulting expression for the cumulative distribution fucntion is as follows:

$$F(T) = 1 - e^{-\left(\frac{T}{\eta}\right)^{\beta}} \qquad (4)$$

From derivations shown in the appendix, rearrangement of equation (9) yields:

$$\ln\ln\left[\frac{1}{1-F(T)}\right] = \beta \ln T - \beta \ln \eta \qquad (5)$$

The two parameters (β, η) can be evaluated from the slope of the linear $\ln\{\ln[1/(1\text{-}F(T))]\}$ *vs.* $\ln T$ Weibull probability plot and from the intercept on the $\ln\{\ln[1/(1\text{-}F(T))]\}$ axis, respectively. Figure 5.9 presents the distribution function, *F(T)*, of percentage-fullerene-coverage for quartz substrates. In this figure, *F(T)* was determined using the *Mean Rank Method* described earlier. Accordingly, the expression used is:

$$F(T) = \frac{\bar{C}(T)}{1 + \bar{C}(T_\infty)} \qquad (6)$$

Where $\bar{C}(T)$ and $\bar{C}(T_\infty)$ are the mean values of percentage-fullerene-coverage at given temperature, T, and at a sufficiently high temperature (note: $\bar{C}(T_\infty) = 100\%$).

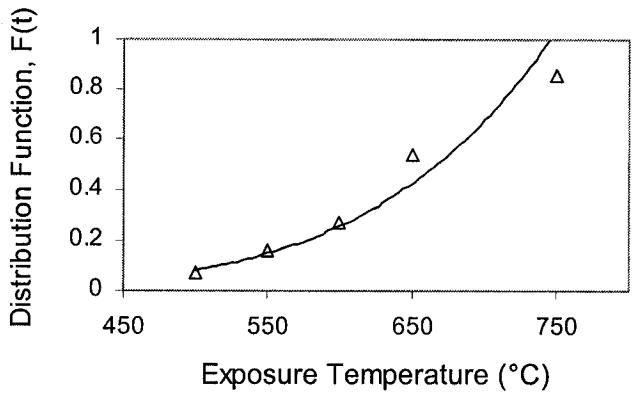

Fig 5.9: Distribution function of percentage-fullerene coverage on quartz disc

From the distribution function, *F(T)*, experimentally determined and presented in Fig. 5.10, a Weibull probability plot of percentage-fullerene-coverage was obtained, based on equation (10), and the result is demonstrated in figure 5.10.

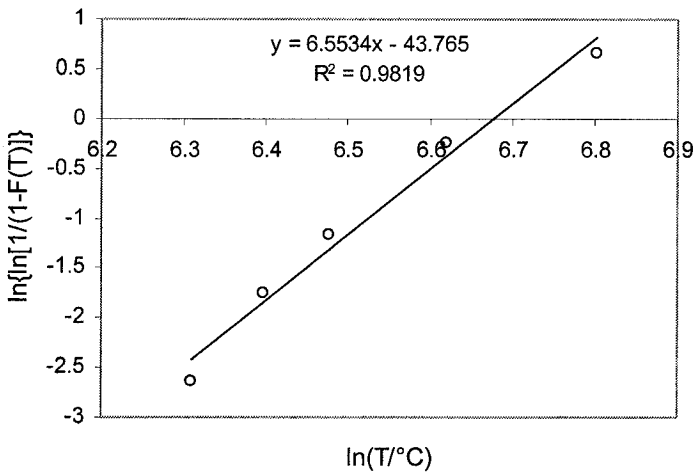

Fig 5.10: Weibull probability plot of percentage-fullerene-coverage on quartz

The plot shows a good straight line, and the shape (β) and scale (η) parameters are evaluated to be 6.5534 and 794.9. From this, our resulting expression for the two-parameter Weibull distribution can be stated as:

$$F(T) = 1 - e^{-\left(\frac{T}{794.9}\right)^{6.5534}} \qquad (7)$$

This allows us to predict the percentage coverage at varying sublimation temperatures for a fixed deposition time of 10 minutes. From first principles, we can obtain the percentage coverage increase rate with respect to sublimation temperature from the following equation:

$$\%Coverage\ increase\ rate = \left(\frac{\beta}{\eta}\right) * \left(\frac{T}{\eta}\right)^{\beta-1} \qquad (8)$$

When this is plotted with respect to temperature, an exponential relation is observed, as shown in figure 5.11.

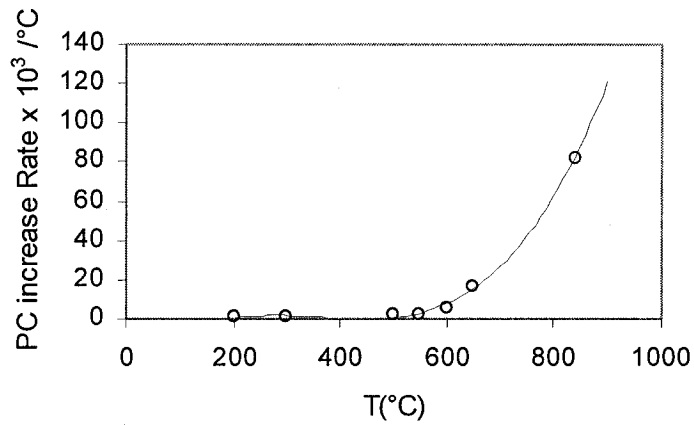

Fig 5.11: Percentage coverage increase rate with respect to sublimation temperature

Since all observations were made for the same deposition time, the results presented on Fig. 5.11 actually correlate with the flux of particles impinging on the substrate which, in turn, is linked to the flux of sublimated particles. Under vacuum conditions (no mass transfer limitation) the flux of particles being vaporized from a surface, Γ_{vapor}, is directly proportional to the material's vapor pressure, p_S, at the temperature of interest, T_S [91]:

$$\Gamma_{vapor} = \frac{p_S}{4(mk_BT_s/3)^{1/2}} \qquad (9)$$

The strong increase of the percent coverage with the sublimation temperature thus reveals a strong temperature dependence for the C_{60} vapor pressure curve, which has a shape that appears, at least at first glance, not different from any other solid material. This

observation corroborate the study of [73] and confirm one of our working hypotheses (section 4.1).

5.4 TRANSMISSION ELECTRON MICROSCOPY (TEM) IMAGES

In order to investigate the effects of the reactive ethane plasma on in-flight sublimated particles, samples of treated fullerenes were collected from the reactor walls around the electrode region and analyzed under a TEM. Untreated, as-received samples were also analyzed and figure 5.12 shows the contrasting morphological differences between the two samples. As can be seen from the TEM images of the untreated samples (fig. 5.12(A-C)), there is significant agglomeration of the particles with no distinct features resulting in plate-like structures. In contrast, fig. 5.12 (D-F) reveal well-defined fullerene nanoparticles of sizes ranging from 30 to 50 nm and isolated from each other by a translucent coating. Such coatings were observed on amorphous SiO_2 nanoparticles treated in a capacitively-coupled rf ethane plasma similar to the one used in the current project and it was determined that this coating contains polymer-like C:H hydrocarbons [76].

Since the nanoparticles are isolated from each other by a translucent layer, it can be deduced that the coating formation process is initiated in-flight, while the nanoclusters are being formed, and before the nanoparticles are deposited on the wall. If that were not the case, polymerization of the C_{60} into larger structures would have occurred. This observation leads to believe that the sublimated, de-agglomerated fullerene molecules, when exposed to a reactive ethane plasma, rapidly acquire a polymer coating. It is also suspected that the coating of the fullerene nanoparticle surfaces by the organic groups leads to a reduction of the surface energy (which is an inherent property of the material being used [62]) and, consequently, to the inhibition of the agglomeration process. Figure 5.13 depicts further images captured from different samples obtained from the reactor. They show similar features as those shown in Figure 5.12. The image of interest has two regions red-boxed to show the contrasting difference between an untreated and a treated sample.

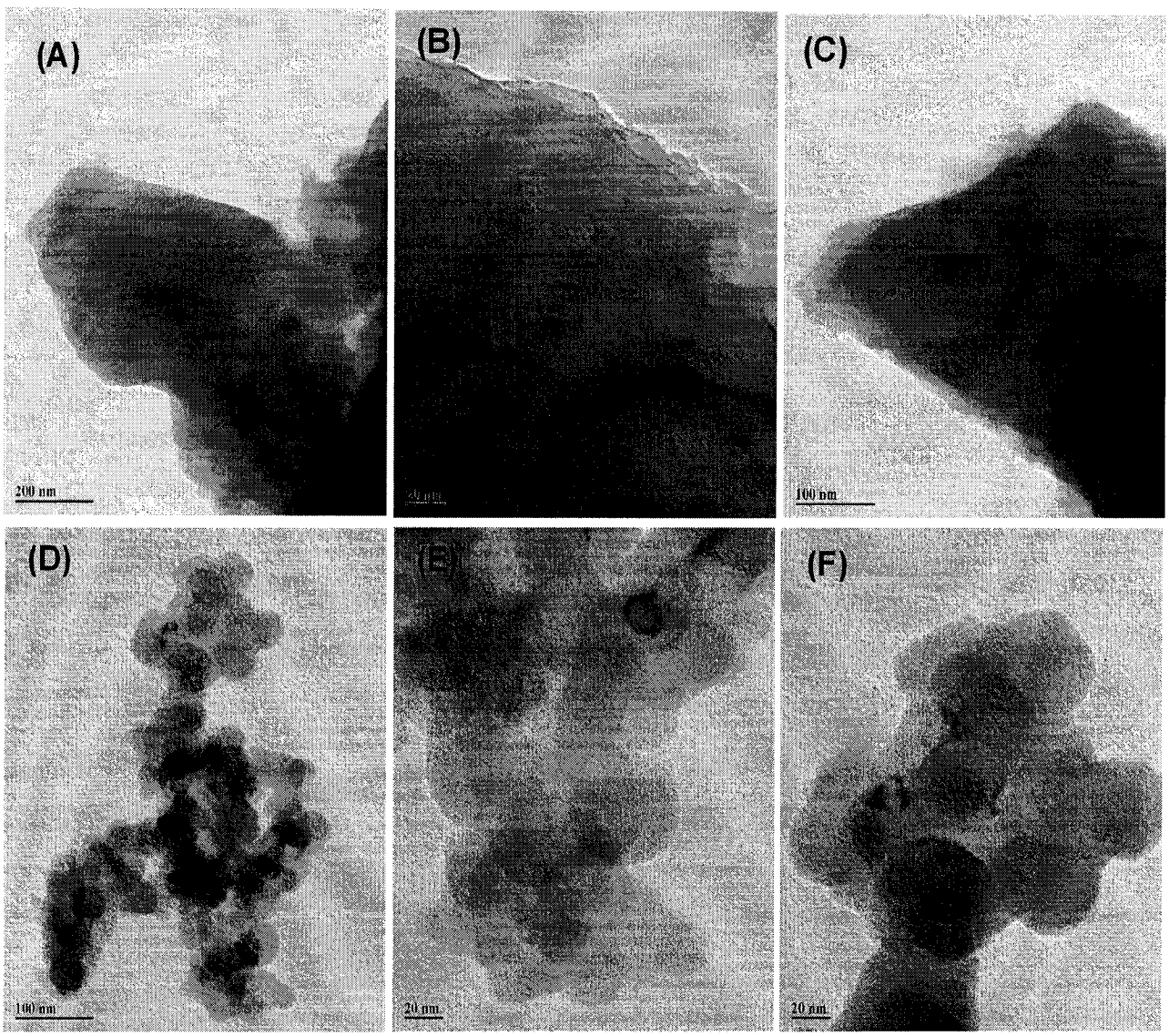

Fig 5.12: (A-C) TEM images of untreated fullerene samples; (D-F) TEM images of treated fullerene samples

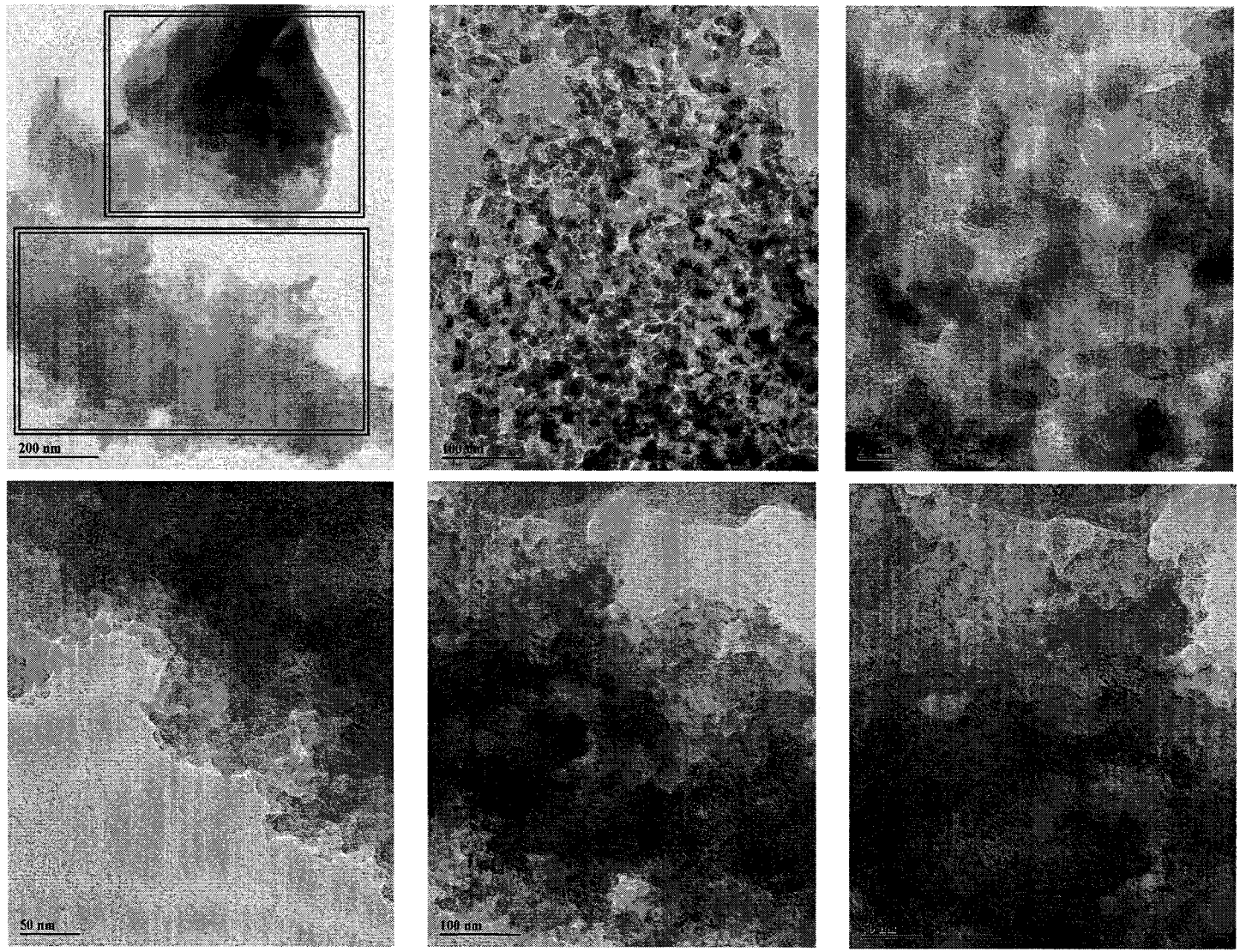

Fig 5.13: Miscellaneous TEM images of treated C_{60} samples obtained from reactor walls around electrode region

5.5 SCANNING ELECTRON MICROSCOPY (SEM) IMAGES

The magnification level attained via optical microscopy is limited by the wavelength of light and, furthermore, some optical contrast is required between the phases. Electron microscopy provides better spatial resolution than optical microscopy, although it is again necessary that there is contrast between the phases [92]. SEM images were obtained of the plasma polymerized polyethylene films as well as the fullerene films. The first set of figures, figure 5.14, show images of polymer films obtained after a deposition time of 15 minutes at an input power of 30 watts, operating pressure of 1 torr and monomer flow rate of 25 sccm.

As can be seen, the polymer films have distinct island-like formations that seem to have percolated to give a uniform film-like morphology on the macroscopic scale. The mean grain size of the island like features is roughly 10 nm. These would be observed in SEM images of all films consisting of a polymer coating.

The crack-like artifacts observed in the images are primarily due to the gold-palladium coating that had to be applied to the substrate prior to analyzing them under the SEM. This is done in order to avoid charge build-up and as the film heats up on being impinged by the electron beam, the artifacts arise due to a difference in thermal expansion coefficients of the metal coating and polymer film.

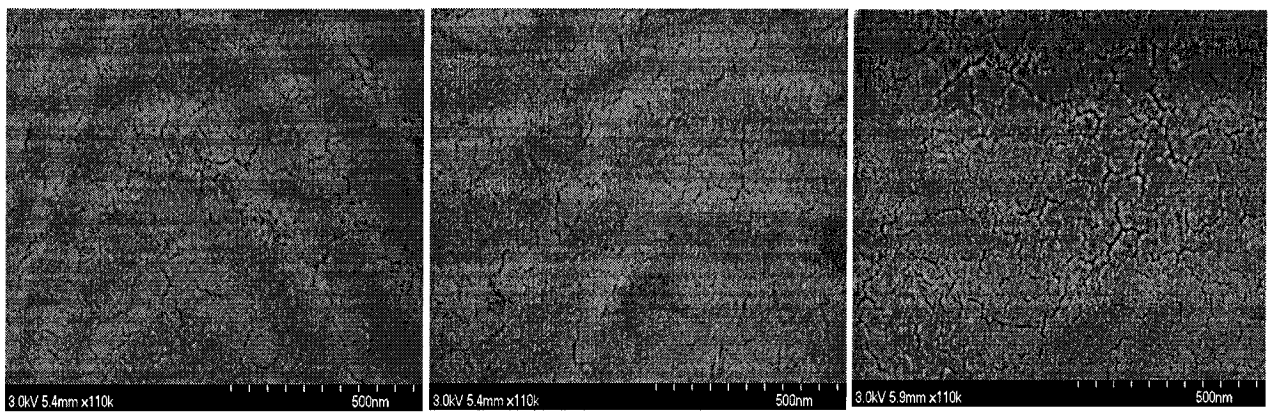

Fig 5.14: SEM images of plasma polymerized polyethylene

The difference in morphology of fullerene + polymer films deposited under different conditions is shown in the SEM micrograph of figure 5.15. Figure 5.15(A) shows a fullerene film obtained via simple sublimation and condensation after exposure to an inert argon plasma. Figure 5.15(B) shows a fullerene film co-deposited in a polymer matrix after exposure to a reactive ethane plasma. In this geometry, the formed nanoparticles have a longer flight time in the plasma while the substrate benefits from a high mass transfer rate due to its perpendicular exposure to the flow. While the treatment of the fullerenes in an inert atmosphere leads to the formation of crystallite-like structures (> 1 μm in size) and several μm-large aggregates, the treatment using ethane gives rise to the formation of 100 to 200 nm-diameter clusters uniformly dispersed over the substrate surface. The nanoclusters appear as aggregate of smaller entities, isolated from each other by the plasma polymerized interlayer. It is difficult to estimate the size of the smaller entities due to the coating, however, their size does not seem to exceed 100 nm. Referring to the observations made from the SEM micrographs, this suggests a thicker coating on the C_{60} nanoparticles as can be expected from a longer residence time in the plasma and a better mass transfer to the substrate. On closer examination of the nanoclusters shown in fig. 5.15(B), it is evident that the morphology of the coating on the nanoclusters themselves is very similar to the coating on the adjacent substrate (fig. 5.15(C) & 5.15(D)). The fact that the nanoclusters appear well-dispersed on the surface is an indication that the clusters are formed prior to impinging on the substrate. Surface diffusion and coalescence of the clusters is not expected to be significant in the present case where the substrate is not heated. It can also be considered that this uniformity is a consequence of the surface charges developed by the clusters in transit in the plasma. Such observations suggest that the PECVD process using the organic monomer C_2H_6 has a dual effect of inhibiting the growth of large C_{60} crystalline structures and the agglomeration of nanoclusters on the substrate. The affect of plasma can be seen twofold as:

(i) it inhibits C_{60} particles from re-agglomerating and growing into crystalline structures due to the negative floating potential they acquire from a build-up of surface charges in situ [92];

(ii) the polymer films deposited on the nanoclusters, which can be seen more clearly at a higher resolution image of fig. 5.15(C) and 5.15(D), could possibly help to reduce the surface energy of the particles, thereby minimizing their tendency to form large agglomerates.

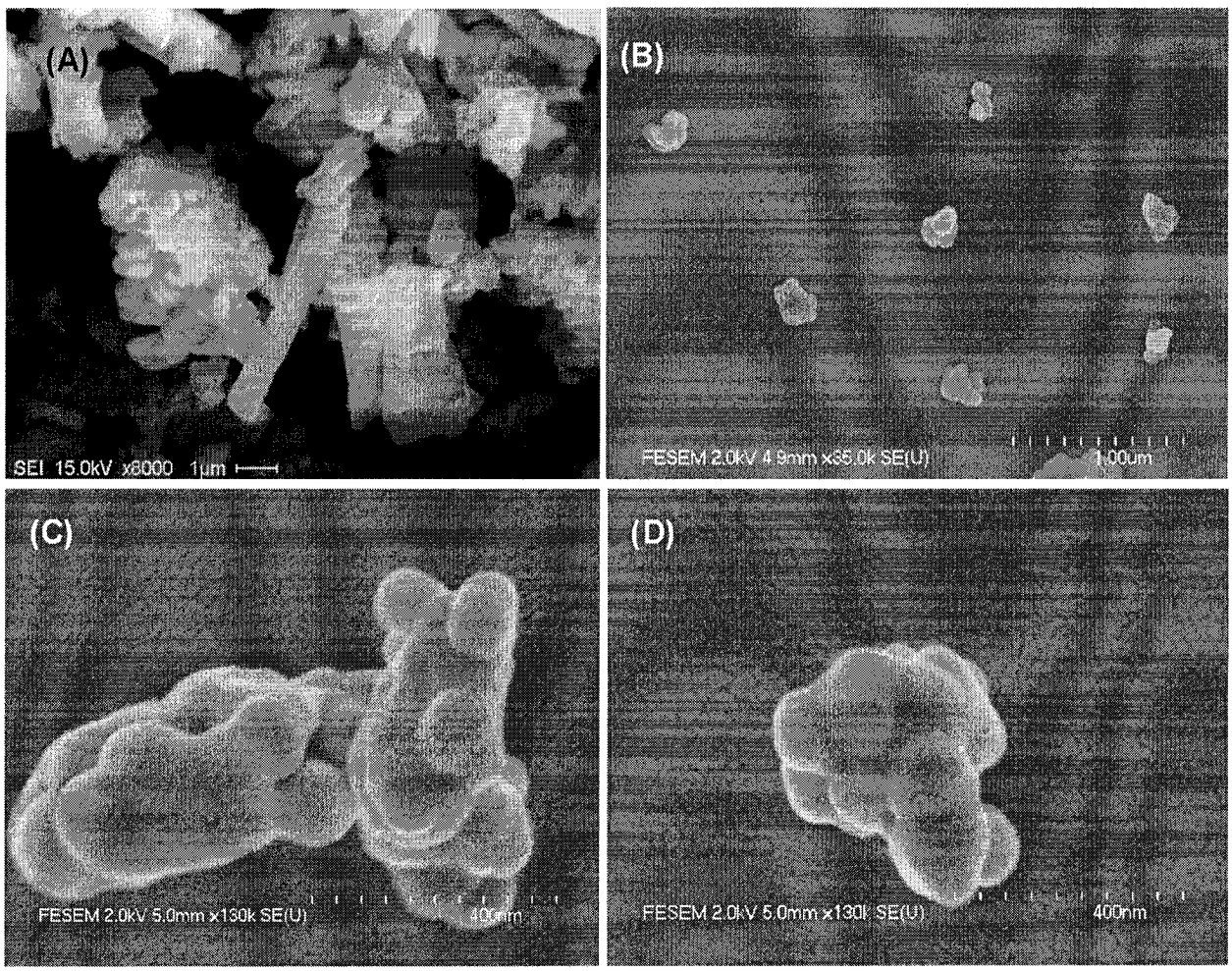

Fig 5.15: (a) SEM image of a fullerene cluster film obtained via simple sublimation and condensation of the fullerene clusters after exposure to a weakly ionized plasma; (b) SEM image of a fullerene cluster film obtained via simple sublimation and condensation of the fullerene clusters and after exposure to a reactive ethane plasma; (c-d) Close-ups of clusters obtained.

Based on previous discussions of the effect of impact energy of clusters on the morphology of the films obtained, it can be inferred that the impact energy of the clusters was well within the low-energy regime (< 0.1 eV/cluster). This is explicable based on the sooty nature of the fullerene films obtained. There is no damage done to the surface

of the substrate and the films consist of a highly porous array of randomly stacked particles.

6 CONCLUSIONS AND RECOMMENDATIONS

Nanomaterials are known to have extremely high surface areas which result in high surface energies reaching the order of 100 kJ/mol for a variety of materials [71]. Due to such high surface energies, nanoparticles naturally agglomerate and can form considerably strong bonds between particles and can therefore not be easily dispersed and are referred to as an aggregate or hard agglomerate.

The unique properties of nanomaterials are often attributable to properties of isolated particles. On combining nanoparticles to a macroscopic work piece, these unique properties are often lost. Therefore, in order to obtain macroscopic parts demonstrating the properties of isolated particles, it is necessary to minimize or avoid interaction of the particles. This is achievable by coating each individual particle with a second layer of polymeric or ceramic material before they are dispersed into the film.

Because of their special composition, these coatings posses a unique combination of properties of the inorganic and organic components (e.g. hydrophobicity, hydrophilicity, anti-fogging, anti-fouling etc) and the particles are then said to have functionalized surfaces. Coated nanoparticles are possibly the only starting material that one can use to produce macroscopic parts exhibiting the unique properties of nanomaterials. These can be produced using plasma processes as the particles leave the plasma zone with high electrical charges of similar sign, thus, avoiding agglomeration [62]. Other gas-phase processes such as the inert gas condensation by Hahn et al. (1988) or the conventional chemical vapour synthesis process by Chang et al (1994) are not capable of producing non-agglomerated nanoparticles.

In this project, an integrated plasma-enhanced chemical vapor deposition system was designed which allows for the synthesis of fullerene C_{60} nanoclusters coated with an

organic coating on exposure of the sublimated C_{60} to a continuous flow ethane plasma sustained by RF capacitive coupling. The system also allows for the deposition of fullerene nanocluster-polymer matrix composite films. Exposure of sublimated C_{60} particles to an organic monomer constitutes a key step in the formation of fullerene nanoclusters and in the dispersion of those nanoclusters in a composite film. The formation of a surface film by an organic group on the fullerene nanoclusters-in-formation, inhibits the natural tendency of the fullerenes to polymerize into large mesoscale (or larger) structures.

During coating, the polymer is introduced as a vapour and the collision frequency increases with the gas pressure. The rate of polymer condensation on the nanoparticle surface may be influenced by many parameters such as electron density, temperature and energy density. In order to achieve a thin and uniform coating on such small nanoparticles, all the synthesis parameters must be optimized. Although a systematic study on the optimization of synthesis parameters has not yet been carried out, previous experimental data [93] has indicated that the coating polymer must be stable and not reactive with the substrate during coating. The gas pressure must be moderate for a low collision rate on the nanoparticle surfaces. In addition, polymerization should take place relatively fast after the condensation on the particle surfaces. This will ensure a uniform coating on the order of 1-2 nm for all particle sizes.

TEM micrographs of the produced nanoclusters reveal that the exposure of fullerene vapors to an ethane plasma leads to the formation of nanoclusters of sizes ranging from 30 to 50 nm, and that a rapid surface-coating of the nanoclusters takes place, inhibiting the polymerization of fullerenes into large mesoscale structures. SEM micrographs of the films deposited on Si substrates placed perpendicular to the nanoclusters/ethane gas stream show plasma polymerized polyethylene films containing well-dispersed and coated fullerene nanoparticles, thus revealing the promise of this process for nanocluster-polymer matrix nanocomposite film production. Lastly, the FTIR spectra of the processed C_{60} show the characteristic peaks of the molecule, strongly suggesting that molecular fragmentation did not occur in the glow discharge.

The currently developed procedure for the synthesis and pre-coating of nanoclusters prior to their incorporation into a matrix to form composite films shows great potential. The process is versatile enough to vary the sublimated fullerene vapor density, the residence time of the vapor in the nanocluster formation zone, and the film formation conditions on a remote surface. Also, the surface chemistry of the nanoclusters can be changed based on the application need by altering the monomer gas utilized. The process can be compartmentalized to three independent stages: (i) sublimation of the raw material; (ii) coating of sublimated nanoclusters and; (iii) incorporation of coated nanoclusters into the desired matrix. Each of the steps can be isolated and adapted in processing of materials according to individual specifications. Currently, the one-step concept of sublimation and precoating of nanomaterials is being further investigated in a new project aimed at obtaining polymer coated aluminium nanoparticles.

Future recommendations which would bring about better control of nanocluster and composite film morphology are as follows: (i) allowances must be made for substrate biasing as this would allow for the control of the impact energy of the clusters on the substrate surfaces; (ii) the substrate holder should be temperature controlled in order to regulate the morphology of the thin film obtains and; (iii) a mechanical shutter should be installed in the particle injector in order to modulate the sublimate flux.

REFERENCES

1- M. Avella et al.; *Appl. Organometal. Chem.*; **2001**; 15: 435-439

2- J. E. Mark et al.; *Polym. Eng. Sci.*; **1996**; 35: 2905

3- B. M. Novak et al.; *Adv. Mater*; **1993**; 5: 839

4- A. J. Kinloch et al.; *Adhesion and Adhesives.*; **1987**; Chapman and Hall, London

5- H. Salmang et al.; *Keramik (part 1).*; **1982**; Springer, Berlin

6- Yu Lipatov et al.; *Adv. Colloid Interface Sci.*; **1979**; 11: 196

7- H. Ushi et al.; *International Symposium on Electrical Insulating Materials*; **1998**; E3-1: 577-582

8- H. Yasuda et al.; *Plasma Polymerization*; **1985**; 3

9- H. Kersten et al.; *Contrib. Plasma Physics*; **2001**; 41: 598-609

10- J. F. Pierson et al.; *Applied Surface Science*; **2001**; 172: 285-294

11- B. M. Smirnov et al.; *Physics of Ionized Gases*; **2001**; John Wiley & Sons, Inc.

12- R. F. Bunshah et al.; *Deposition Technologies of Films and Coatings*; **1994**; Noyes Publications

13- J. R. Roth; *Industrial Plasma Engineering*; **2001**; 2; IoP Publishing

14- R. J. Goldston, *Introduction to Plasma Physics*, **1997**

15- Grill, A; *Cold plasmas in materials fabrication: from fundamentals to applications*; **1994**; IEEE Pres – New York

16- A. Bell; *The Applications of Plasmas to Chemical Processing*; **1967**; MIT Press

17- M. Capitelli; *Plasma Technology, fundamental applications*; New York; 59-80

18- J. L. Vossen; *Thin Film Processes*; **1978**; New York: Academic Press

19- D. W. Hess; *Microelectronics Processesing*; **1989**; Washington DC: American Chemical Society, 377

20- Y. Catherine; *In Plasma Processing*; **1985**; 317

21- U.S. Federal Communications Commission Rules and Regulations. Washington, DC: U.S. Government Printing Office; **1964**

22- J. R. Roth; *Industrial Plasma Engineering*; **1995**; 1; IoP

23- N. Mayo et al.; *Appl. Phys.*; **1984**; 55; 4404

24- A. Grill et al.; *Surf. Coat. Technol.*;**1990**; 43/44; 745

25- J. W. Coburn; *J. Vac. Technol.*; **1979**; 16; 371

26- A. Kubono; *Prog. Polym. Sci*; **1994**; 19; 389

27- W. Gombotz et al; *J. Appl. Polym. Sci.: Appl. Polym. Symp.*; **1988**; 285

28- F. F. Shi; *Surface Coatings Technology*; **1996**; 82; 1-15

29- H. Yasuda; *J. Membr. Sci.*; **1989**; 46; 1

30- H. Yasuda; *Plasma Polymerization*; **1985**; New York: Academic Press

31- A. T. Bell; *Topics in Current Chemistry, Plasma Chemistry III*; **1980**; Berlin: Springer-Verlag; 43

32- H. U. Poll; *Eur. Polym. J.*; **1976**; 12; 505

33- H. Yasuda; *Thin Film Processes*; **1978**; New York: Academic Press

34- A. Hiratsuka et al; *Electroanalysis*; **2000**; 9; 12

35- F. F. Shi; *Surface Coatings Technology*; **1996**; 82; 1-15

36- A. Hiratsuka et al; *Electroanalysis*; **2000**; 9; 12

37- E. E. Johnston et al; *J. Electron Spectroscopy and Related Phenomena*; **1996**; 81; 23

38- H. Yasuda; *J. Appl. Polym. Sci.*; **1979**; 23; 3449

39- H. Yasuda; *J. Polym.. Sci.*; **1978**; 16; 743

40- S. Y. Park et al.; *Plasma Polymerization and Plasma Interactions with Polymeric materials*; **1990**; New York: John Wiley & Sons; 91

41- A. M. Rao et al., *Science*, **1993**

42- C. Yeretzian et al., *Nature*, **1992**

43- Y. B. Zhao et al., *Appl. Phys. Lett.*, vol. 64, **1994**

44- N. Takahashi et al., *J. Appl. Phys.*, vol 74, **1993**

45- H. Yamawaki et al., *J. Phys. Chem.*, vol. 97, **1993**

46- S. Pekker et al., *Science*, vol 265, **1994**

47- M.S. Dresselhaus et al., *Science of Fullerenes and Carbon Nanotubes*, Academic Press, New York, NY **1996**

48- Y. Wang, *Nature (London)*, **1992**

49- C. Binns; *Surface Science Reports*; **2001**; 44; 1-49

50- K. Sattler et al.; *Phys. Rev. Lett.*; **1980**; 45; 821

51- T. G. Dietz et al.; *J. Chem. Phys*; **1981**; 74; 6511

52- J. Gspann; *Nucl. Instrum. Meth.*; **1989**; B 37/38; 775

53- J. Gspann; *Nucl. Instrum. Meth.*; **1993**; B 80/81; 1336

54- W. Habrich et al.; *Metal Clusters at Surfaces*; **2000**; Springer, Berlin

55- H. Haberland et al.; *Phys. Rev.*; **1995**; B 51; 11061

56- J. Musil; *Surface Coatings Technology*; **2000**; 125; 322

57- L. Maya et al.; *J. Vac. Sci. Technol.*; **1995**; B 13; 361

58- M. Diserens; *Surface Coatings Technology*; **1999**; 120; 118

59- J. Musil; *Surface Coatings Technology*; **1999**; 115; 32

60- S. Veprek et al.; *Thin Solid Films*; **1995**; 268; 64

61- M. K. Corbierre et al.; *J. Am. Chem. Soc.*; **2001**; 123; 10411

62- D. Votollah et al.; *Journal of Nanoparticle Research*; **1999**; 1; 235-242

63- R.W. Siegel, *Nanostruct. Mater.*,3, 1, **1993**

64- G.C. Hadjipanayis and R.W. Siegel, *Nanophase Materials,Synthesis-Properties Applications* (Kluwer Press, Dordrecht, The Netherlands, **1994**

65- G.M. Whitesides, J.P. Mathias, and C.T. Seto, *Science,* 254, 1312, **1991**

66- C.D. Stucky and J.E. MacDougall, *Science*, 247, 669, **1990**

67- H. Gleiter, *Nanostruct. Mater.,* 6, 3, **1995**

68- *Nanotechnology,* edited by A.T. Wolde (STT Netherlands Study Center for Technology Trends, The Hague, The Netherlands, **1998**

69- N. Inagaki, S. Tasaka, and K. Ishii, *J. Appl. Polym. Sci.*, 48, 1433, **1993**

70- C. Bayer, M. Karches, A. Mattews, and P.R. Von Rohr, *Chem. Eng. Technol.*, 21, 427, **1998**

71- R. He, *Mat. Res. Soc. Symp. Proc. Vol. 703*, **2002**

72- R. Enrique et al.; *Surface Coatings Technology*; **2002**; 150; 1-7

73- M. V. Korobov, E. V. Skokan, D. Yu. Borisova and L. M. Khomich, *Russian J. Phys. Chem.*; **1996**; 70, 926

74- C. Giusca, M. Baibarac, S. Lefrant, O. Chauvet, I. Baltog, A. Devenyi and R. Manaila, *Carbon*; **2002**; 40, 1565

75- H. Kersten, H. Deutsch, M. Otte, G. H. P. M. Swinkels and G. M. W. Kroesen, *Thin Solid Films*; **2000**; 377-378, 530

76- A. Kouprine, F. Gitzhofer, M. I. Boulos and A. Fridman, *Plasma Chem. Plasma Process*; **2004**; 24, 189

77- G. Akovali; *J. Appl. Poly. Sci.*; **1986**; 32; 4027-4042]

78- H. Hiratsuka; *J. Appl. Poly. Sci.*; **1978**; 22; 917-925

79- de Heer et al.; *Solid State Physics*; **1987**; 40; 93

80- H. Hiratsuka et al.; *J. App. Poly. Sci.*; **1978**; 22; 917-925

81- H. Kobayashi; *Macromolecules*; **1974**; 7; 277

82- H. Kobayashi; *J. Appl. Polym, Sci.*; **1973**; 18; 885

83- Harick, N.J., *Internal Reflection Spectroscopy*, Wiley-Interscience: New York, **1967**

84- A. M. Dorfman, *Physical-Technical Institute*, Russian Federation, **2003**

85- C. A. Reed, *Chem. Rev.*, 100, 1075-1120, **2000**

86- Abrefah et. Al, *Appl. Ohys. Lett.*, Vol. 60, No. 11, **1992**

87- B. L. Vlcek, *National Aeronautics and Space Administration*, **2002**

88- W. D. Bowen, *ICES J. of Marine Sci.*, 60, **2003**

89- H. Zang, *Computers in Railways IX*, **2004**

90- http://www.itl.nist.gov/div898/handbook/eda/section3/eda364.htm#FORMULAS

91- S. Coulombe, *PhD Thesis, McGill University*, 1997

92- A. Garton, *Polym. Eng. and Sci.*, 1982

93- D. Shi, *J. Mater. Res.*, Vol. 17, No. 10, **2002**

APPENDIX

METHODS FOR PARAMETER ESTIMATION

The following is an exposition of some common methods utilized for the estimation of Weibull parameters, namely: the *shape parameter* (β); and the *scale parameter* (η). They are classified into two categorical methods: graphical and analytical.

1 Graphical Methods

Graphical methods are commonly utilized due to their simplicity and rapid computational procedures. However, this is at the expense of involving a greater probability of error. Two of the main graphical methods are described as follows.

1.1 Weibull Probability Plotting

The Weibull distribution density function (Mann, N. R., Schafer, R. E., and Singpurwalla, N. D., *Methods for statistical analysis of reliability and life data*, **1974**, John Wiley and Sons, New York) is given by the following equation:

$$f(x)=\frac{\beta}{\eta}\left(\frac{x-\gamma}{\eta}\right)^{\beta-1} e^{-\left(\frac{x-\gamma}{\eta}\right)^{\beta}}, \quad \beta>0,\eta>0,x\geq\gamma\geq 0 \tag{1}$$

The cumulative Weibull distribution function is given by:

$$F(x)=1-e^{-\left(\frac{x-\gamma}{\eta}\right)^{\beta}} \tag{2}$$

where; β is the shape parameter, η is the scale parameter, and γ is the location parameter. In order to obtain the relation between the cumulative distribution function (CDF) and the two parameters (β,η), a double logarithmic transformation is taken of the CDF. Letting $\gamma=0$ from (2), we have:

$$1-F(x)=e^{-\left(\frac{x}{\eta}\right)^{\beta}} \tag{3}$$

$$\frac{1}{1-F(x)} = e^{\left(\frac{x}{\eta}\right)^{\beta}} \qquad (2)$$

$$\ln\left[\frac{1}{1-F(x)}\right] = \left(\frac{x}{\eta}\right)^{\beta}$$

$$\ln\ln\left[\frac{1}{1-F(x)}\right] = \beta \ln x - \beta \ln \eta$$

The last equation is of a straight line and in order to plot $F(x)$ versus x, the following algorithm is to be applied:

1- Rank the observations in ascending order

2- Estimate $F(x_i)$ of the i^{th} rank of observation

3- Plot $F(x_i)$ vs. x in the Weibull probability paper

The values for $F(x_i)$ in 2 and 3 may be estimated by using one of the methods presented in the following table (where n is the total number of data points).

Table A.1: Methods for estimating $F(x_i)$

Method	$F(x_i)$
Mean Rank	$\frac{i}{n+1}$
Median Rank	$\frac{i-0.3}{n+0.4}$
Symmetrical CDF	$\frac{i-0.5}{n}$

1.2 Hazard Plotting Technique

This is an estimation procedure for the Weibull parameters. This is done by plotting the hazard function $H(x)$ against the *observations* on a hazard paper or a simple log-paper. The hazard function is as follows:

$$h(x)=\frac{\beta}{\eta}\left(\frac{x}{\eta}\right)^{\beta-1}$$

The cumulative hazard function is as follows:

$$H(x)=\int h(x)=\left(\frac{x}{\eta}\right)^{\beta} \qquad (3)$$

Equation (3) can be transformed by taking the natural logarithm as follows:

$$\ln H(x)=\beta\{\ln x-\ln\eta\}$$

$$\ln x=\frac{1}{\beta}\ln H(x)+\ln\eta \qquad (4)$$

From (4), $\ln H(x)$ versus $\ln x$ can be plotted using the following procedure:

1- Rank the observations in ascending order

2- For each observation, calculate $\Delta H_i=\frac{1}{(n+1)-1}$

3- For each observation, calculate $H=\Delta H_{1+}\Delta H_2+\ldots+\Delta H_i$

4- Plot *ln H* vs. *ln x*

5- Fit a straight line

Upon completion of plotting, the estimated parameters are:

$$\beta=\frac{x}{y}=\frac{1}{slope}$$

at $H=1$, $\eta=x$

2 Analytical Methods

Due to the high probability of error in using graphical procedures, analytical methods are commonly preferred. The following is the most commonly applied analytical technique in engineering and analytical problems.

2.1 Least Squares Method (LSM)

In this technique, it is assumed that a linear relation exists between the two variables of interest. For Weibull parameter estimation, the method of *least squares* is utilized and applied to the results from the previous section. Recall that:

$$\ln\ln\left[\frac{1}{1-F(x)}\right]=\beta\ln x-\beta\ln\eta \tag{5}$$

Equation (5) is a linear equation. It can thus be written that

$$\bar{x}=\frac{1}{n}\sum_{i=1}^{n}\ln\left\{\ln\left[\frac{1}{(1-\frac{i}{n+1})}\right]\right\} \tag{6}$$

$$\bar{y}=\frac{1}{n}\sum_{i=1}^{n}\ln x_i \tag{7}$$

$$\hat{\beta}=\frac{\left\{n\cdot\sum_{i=1}^{n}(\ln x_i)\cdot(\sum_{i=1}^{n}\ln\left\{\ln\left[\frac{1}{(1-\frac{i}{n+1})}\right]\right\})\right\}-\left\{\sum_{i=1}^{n}\ln\left\{\ln\left[\frac{1}{(1-\frac{i}{n+1})}\right]\right\}\cdot\sum_{i=1}^{n}\ln x_i\right\}}{\left\{n\cdot\sum_{i=1}^{n}(\ln x_i)^2\right\}-\left\{\sum_{i=1}^{n}(\ln x_i)\right\}^2} \tag{8}$$

From equations (5) – (8), the estimates of β and η can be calculated.